Evaluating spatial and temporal dynamics of river-floodplain connectivity using hydrometric, geochemical and microbial indicators.

Alexander C. Brooks [1]
Tim Covino [1,2]
Ed K. Hall [1,2]

[1.] Department of Ecosystem Science and Sustainability, Colorado State University, Fort Collins, Colorado, 80524, USA
[2.] Natural Resources Ecology Laboratory, Colorado State University, Fort Collins, 80524, USA

Corresponding Author: Alexander C. Brooks, alex.brooks@colostate.edu

Orcid IDs:

Alexander Brooks: https://orcid.org/0000-0001-9742-4149

Tim Covino: https://orcid.org/0000-0001-7218-4927

Ed Hall: https://orcid.org/0000-0001-8004-246X

Key Points

- Measures of hydrologic connectivity are necessary to understand river-floodplain condition and function
- We develop continuous measures of hydrologic connectivity across space and time in a river-floodplain system
- We observed the greatest heterogeneity in river-floodplain connectivity at moderate flows

Abstract

Water-mediated linkages that connect landscape components are collectively referred to as hydrologic connectivity. In river-floodplain systems, quantifying hydrologic connectivity enables descriptions of hydrologic function that emerge from complex, heterogeneous interactions of underlying geomorphic, climatic and biologic controls. Here, we measure hydrologic connectivity using field indicators and develop a continuous connectivity metric that represents a vector strength between a source along the North St Vrain river to ten surface water target sites within the river-floodplain system. To measure this connectivity strength, we analyzed hydrometric, injected conservative tracers, and natural occurring geochemical and microbial indicators across streamflows in 2018. We developed empirical models of hydrologic connectivity as a function of river stage to predict daily connectivity strength across multiple floodplain sites for five years between May and September of 2016-2020. Three sites were either consistently connected or disconnected to the river, while seven varied across time in their hydrologic connectivity strength. Of the sites with variable connectivity, some disconnected very quickly and others had a prolonged disconnection phase. By scaling site dynamics to the system scale, we found across-system hydrologic connectivity always increased with streamflow while across-system variance in hydrologic connectivity peaked at intermediate streamflow. At sites with intermittent connections to the river, river stage disconnection thresholds were variable (308 to 650 mm) and their connectivity dynamics were sensitive to inter-annual variation in streamflows, suggesting that future connectivity behavior under climate change will depend on how flow durations change across a range of flow states.

1. Introduction

Hydrologic linkages of matter and energy within landscapes are important regulators of physical, biogeochemical (Covino, 2017) and biological processes (Amoros & Bornette, 2002). These linkages, defined as hydrologic connectivity, are a fundamental landscape property that connect multiple landscape components (e.g., uplands, streams, floodplains, hyporheic zones, groundwater). Hydrologic connectivity emerges from complex interactions of topographic, climatic, geologic, biotic, and anthropogenic controls (Leibowitz et al., 2018). Recently, hydrologic connectivity has gained popularity as a conceptual and quantitative framework because it enables description of emergent patterns in hydrologic function without requiring the full quantification of underlying processes and controls (Wohl et al., 2019).

River-floodplain systems are distinct landscapes formed by interactions between rivers and adjacent landforms that support important ecologic and hydrologic services (Opperman et al., 2010). Surficial flow and flood pulses from rivers to their floodplains (Junk et al., 1989; Tockner et al., 2000) as well as subsurface hyporheic exchange shape the geomorphic structure of both the river and the floodplain (Stanford & Ward, 1993). This generates spatially heterogeneous landscapes with a mosaic of habitats each with distinct hydrologic regimes (Poole, 2002). Return flows from floodplains to rivers partially regulate downstream physio-chemistry including fluxes and concentrations of organic matter, sediment, nutrients and heavy metals (Bellmore & Baxter, 2014; Briggs et al., 2019; Tockner et al., 2002; Wohl et al., 2017). Despite their benefits, in many systems, hydrologic connections in river-floodplains have been altered due to water management of river systems and cultivation and development within floodplain areas (Tockner & Stanford, 2002). As efforts have grown to restore connections between rivers and their floodplains, so has the need to effectively characterize hydrologic dynamics, which remains challenging given the spatial and temporal heterogeneity within these systems (Roni et al., 2019).

Measuring hydrologic connectivity in river-floodplain systems can be useful because it describes emergent hydrologic behavior without fully quantifying underlying interactions. In river-floodplain systems, hydrologic connections operate simultaneously across multiple dimensions: vertical (surface-groundwater), lateral (river-floodplain & floodplain-hillslope), longitudinal (upstream to downstream), and temporal (J. V. Ward, 1989). The magnitude and directionality of connectivity can vary depending on the spatial and temporal scale being considered (Covino, 2017). Equally as important as identifying when

landscape features are connected by surface and sub-surface pathways is identifying when they are not connected, known as disconnectivity or isolation, which at landscape scales plays a critical role in a suite of important hydrologic and biogeochemical processes (Cohen et al., 2016; Rains et al., 2016), water chemistry (Cheng & Basu, 2017), and in the maintenance of habitat complexity and biodiversity (Amoros & Bornette, 2002).

1.1 Quantifying Hydrologic Connectivity in River-Floodplain Systems

The physical template that determines potential connective pathways in river-floodplain systems is known as structural connectivity (Bracken & Croke, 2007). In river-floodplain systems, analyses of digital elevation models and/or habitat features is common for identifying surficial structural connections, while identification of physical subsurface structural connections is more limited given subsurface heterogeneity and often requires broad simplifications of underlying complexity (K. L. Jones et al., 2008; Thoms et al., 2005; A. S. Ward et al., 2012). Functional hydrologic connectivity refers to the degree that material and/or energy is transferred within the landscape. For functional hydrologic connectivity (hereafter connectivity) to be achieved, flow must overcome resistance, impedances, and losses along structurally connected pathways (Ali et al., 2018). Thus, connectivity within river-floodplain systems may only occur under specific hydrologic conditions driven by internal (e.g., antecedent moisture conditions and geomorphic structure) and external (e.g., river flow state, local precipitation) factors (Fritz et al., 2018).

Assessing functional connectivity requires an approach that can quantify the degree to which material and energy moves among landscape components (Bracken et al., 2013; Turnbull et al., 2008). One common approach is to use hydrodynamic models and topographic data to predict connectivity dynamics (Chen et al., 2020; Stone et al., 2017). However, developing accurate models can be challenging because both the models and the underlying topographic datasets often miss do not capture the small scale geomorphic features and processes that are critical drivers of lateral connectivity (e.g., log jam development and failure) (Addy & Wilkinson, 2019). Therefore, field methods that capture spatiotemporal patterns in functional connectivity are also valuable. Common field methods to measure functional connectivity between rivers and their floodplains include hydrologic measurements (e.g., soil moisture,

101 water levels, streamflow), geochemical and isotopic end-member mixing analyses and conservative tracer
102 experiments (Cabezas et al., 2011; C. N. Jones et al., 2014; Rinderer et al., 2018).

103 The field methods listed above tend to provide information about different aspects of connectivity and
104 are often only applicable at specific spatial or temporal scales, hindering between-study comparisons and
105 the direct translation of connectivity assessments to policy and management decisions (Wohl et al.,
106 2019). Additionally, connectivity is often considered as a categorical or binary attribute (i.e., connected or
107 isolated) where connectivity is achieved when river stage is above a specific threshold or when physio-
108 chemical states are similar between two landscape components with a known structural connection.
109 However, fluvial networks such as river-floodplain systems also experience gradients in hydrologic
110 conditions, suggesting continuous metrics of connectivity may more accurately describe system level
111 properties (Garbin et al., 2019).

112 *1.1.1 Incorporating Microbial Indicators of Hydrologic Connectivity*

113 One emerging field-based approach that may provide new insights into connectivity is utilizing hydrologic
114 information contained in microbiomes. Recent work has demonstrated that analysis of microorganisms
115 can be a valuable tool in hydrologic research because membership of aquatic microbiomes are intimately
116 coupled with hydrologic processes (Good et al., 2018; Martínez-Carreras et al., 2015; Pfister et al., 2009).
117 Microorganisms are passive dispersers in aquatic systems and dispersal effects are primarily driven by
118 the directional flow of water (Nemergut et al., 2013). As a result, membership of downstream aquatic
119 microbiomes have been shown to be similar to the microbiomes within shallow soils (Crump et al., 2012)
120 and deeper groundwaters (Amalfitano et al., 2014) that generate streamflow. However, as surface water
121 ecosystems become disconnected and residence times of aquatic systems increase, community
122 assembly is increasingly affected by ecological dynamics (e.g., competition, predation) that result in
123 changes in membership of the site-specific microbiome (Crump et al., 2012; Lindström et al., 2006). At
124 any one point in time, aquatic microbiome membership is the balance between immigration and
125 emigration, which are primarily regulated by hydrologic connectivity, and microbial growth and mortality,
126 which are affected by *in situ* environmental parameters (e.g., resources and temperature) (Crump &
127 Hobbie, 2005; Read et al., 2014; Savio et al., 2015). As hydrologic flow states and aquatic network

structure also influence hydrologic connectivity, the membership of aquatic microbiomes has the potential to reflect connectivity status. The recent formalization of analytical techniques and bioinformatic pipelines to characterize microbiome membership have made analyses of environmental microbiomes more affordable and accessible to non-specialists (Thompson et al., 2017). These increasingly routine analyses of microbiome membership, coupled with the ubiquity of microorganisms, make microbial analyses a potentially powerful tool for assessments of hydrologic connectivity.

1.2 Study Overview

In this study we quantified temporal patterns of hydrologic connections as a continuous value between 0 and 1 from a source (the river at the upstream boundary of the study system, see Figure 1) to target sites (sites located both on the floodplain and downstream on major channel braids of the river, see Figure 1). To do this, we combined data from a network of continuous water level sensors, conservative tracer injections, and weekly sampling for aqueous geochemistry and microbiome membership in order to quantify connectivity of surface water features within the montane river-floodplain system. We also assessed the potential for microbiomes to be used as indicators of connectivity strength and identify whether they provide complementary information to more traditional hydrologic and geochemical connectivity indicators. We then generate site-specific empirical models of connectivity strength for each target site based on streamflow at the source and predict daily connectivity strength at each site. From this developed connectivity dataset, we seek to understand:

1) How does hydrologic connectivity differ within the river-floodplain system?
2) Does connectivity demonstrate binary or continuous behavior?
3) How does site-level connectivity aggregate to system-wide dynamics?
4) How sensitive is floodplain connectivity to inter-annual variability in streamflow?

2. Methods

2.1 Site Description

This study was conducted within a river-floodplain system along the North St. Vrain River, Colorado (Figure 1). The river drains an 84km^2 watershed within Rocky Mountain National Park and has a

snowmelt driven hydrograph with late spring/early summer snowmelt peak flows and summer streamflow recession (Figure 1). The river has a multi-thread planform within the river-floodplain system which is 1.5km long, 200m to 300m wide with an area of 0.47km^2. The floodplain has high spatial heterogeneity with a mosaic of beaver ponds, side channels and wetlands (Laurel & Wohl, 2019). Beaver colonies are active within the reach and geomorphic structures in the floodplain are strongly impacted by historic and current beaver activities including dam construction, channel dredging and pond creation. The floodplain is vegetated with riparian species including willows (*Salix* spp.), river birch (*Betula* spp.), and quaking aspens (*Populus tremuloides*).

Eleven surface water sites were established within the river-floodplain system (Figure 1b). There were four sites along the river including at the upstream (Inflow) and downstream (Outflow) boundaries of the river-floodplain reach and along two major channel braids within the river-floodplain system (Main-Mid & Main-Braid, see Figure 1). To capture the heterogeneity of aquatic habitats across the floodplain, we included four side channel sites (Side-01 to Side-04), two connected pond sites that had an upstream surface connection to the river (Pond-Con-01 & Pond-Con-02) and one isolated pond (Pond-Iso) with no apparent surface channel connection to the river.

2.2 Hydrometric Field Measurements and Conservative Tracer Injection

At all eleven sites, we monitored water level at 15-minute intervals from May 01, 2018 through September 30, 2018 using either TruTrack Capacitance Rods or HOBO U20L Pressure Transducers. To capture relative stage dynamics, we standardized mean daily stage as a z-score by normalizing mean daily stage by the seasonal (i.e., May-September) mean and standard deviation of water levels across the period of record at each individual site. Precipitation (2018 water year total: 645 mm) and snow water equivalent (2018 peak: 401 mm) records were obtained from the Wild Basin SNOTEL, #1042, (2914 m), located within the watershed.

To determine how river-floodplain connectivity changed as a function of streamflow we conducted instantaneous NaCl injection experiments at high (June 13, 2018) and low flows (July 30, 2018). We injected NaCl into the main stem of the river, 125m upstream from Inflow, and monitored the change in specific conductance (SC) over time (i.e., the breakthrough curve, BTC) at six downstream locations

(Table 1) using Campbell CS547A-L conductivity loggers. We calculated modal velocity (V_m) as the time to peak (TTP) divided by the flow path distance from the injection site ($DIST_f$) to the monitoring site.

2.3 Field Sample Collection and Lab Analysis

At all sites, we collected water samples from May 05, 2018 to September 25, 2018 at approximately weekly intervals for a total of 21 sampling events. A total of 228 water samples were collected for aqueous geochemistry, filtered within 24 hours with a 0.45-µm PVDF filter (Millipore, HVLP04700) and frozen until analysis for major ions using a Dionex ICS-3000 ion chromatograph at the US Forest Service Rocky Mountain Research Station in Fort Collins, Colorado. A subset of 215 water samples were collected in sterile 60 mL falcon tubes for 16S rRNA amplicon analysis, kept cold until filtered within 12 hours onto a white polycarbonate GTTP 0.2-µm filter (Millipore, GTTP02500), flash frozen with liquid nitrogen and then stored in a -80°C freezer until analysis. To assess within site variability, for a subset of sites (Inflow, Outflow, Side-01, Pond-Con-01, and Main-Mid), we collected duplicate samples each week for 16S rRNA analyses. At all other sites, only individual samples were collected. Due to analysis constraints, Side-02 was sampled for 16S rRNA analysis at a bi-weekly frequency while other sites were sampled weekly.

We extracted DNA from each filter with a MoBio PowerSoil® DNA Isolation Kit using standard protocols. The 16S rRNA gene (V4 region) was amplified using 515F and 806R universal primers with the forward primer barcoded following the Earth Microbiome Project protocols (Caporaso et al., 2011). The forward primer 515F included the unique sample barcode following Parada et al. (2016) and both primers included degeneracies as described in Parada et al. (2016) and Apprill et al. (2015). For each sample, we ran a 50 µL PCR reaction using an Invitrogen PlatinumTM Hot Start PCR Master Mix with 10 µL of DNA. The PCR product was quantified and then combined into a single pool in equimolar concentrations and cleaned using a MinElute® PCR Purification kit. Cleaned, pooled DNA was sequenced with a MiSeq reagent v2 500 cycle kit on the Illumina MiSeq platform at the Colorado State University Next Generation Sequencing Core facility. Sequence reads were analyzed using MOTHUR (Schloss et al., 2009) and OTU counts defined at a 97% similarity of the sequence using the OptiClust algorithm. Generated OTUs were then aligned to a SILVA reference file (Quast et al., 2013). We then removed samples with limited

sequences (<1000 reads), trimmed operational taxonomic units (OTUs) to remove samples not observed more than 3 times in 20% of the samples, and relativized OTU counts by the total OTUs in the sample. All 16S amplicon analyses were conducted using the phyloseq package in R (McMurdie & Holmes, 2013). Due to lack of duplication at all sites, we further merged duplicate samples into mean values to simplify subsequent analysis.

2.4 Connectivity Strength Metrics

To quantify hydrologic connectivity, we identified a source site (Inflow) and considered the magnitude of connectivity between this source and multiple target sites. We first analyzed connectivity information using relative stage dynamics. To do so, we used a graphical analysis approach by plotting the mean daily Inflow stage against the relative stage as represented by stage z-scores (described in section 2.2) at the target sites. Strongly co-varying stage levels between source and target may suggest the presence of connectivity while inflection points in source-target stage relationships can help identify thresholds at which connectivity dynamics shift (Cabezas et al., 2011). To identify inflection points in source-target stage relationships and identify inflection thresholds at Inflow (I_{stage}), we fit broken line linear regression models using the segmented package in R, which identifies a user-defined number of inflection points (Muggeo, 2008). Because hysteresis was observed in the source-target relationship at several sites, we removed the rising limb from the inflection point identification process. For improved interpretability, we constrained the analysis to either a linear fit model (zero inflection points) or a one inflection point model and chose the model that minimized the Bayesian information criterion (BIC). In all cases, the single inflection point model was chosen over the linear fit. It should be noted that while coherent hydrologic fluctuations between sites can be a useful tool for confirming connectivity, it can also be subject to false positives when other factors act similarly on both sites (Rinderer et al., 2018).

We developed an approach to quantify the connectivity magnitude between source and target sites using both geochemical and microbial indicators. For both metrics, we quantified the magnitude, defined hereafter as connectivity strength (σ), as a continuous variable ranging from 0 and 1. Connectivity strength denotes the degree of influence of the source on the target. To measure connectivity strength, we assumed that when strong hydrologic connectivity was present, source and target water compositions

would be more similar than when connectivity was weak or absent. This is a commonly used assumption embedded in source water mixing approaches which use aqueous geochemistry to assess hydrologic connectivity (Cabezas et al., 2009; C. N. Jones et al., 2014). For microbial communities, we expected that when hydrologic connectivity was strong, the membership of the water column microbiome would be more similar because the target community would be strongly influenced by immigration from the source community. Conversely, when hydrologic connectivity was weak/absent, we expected inter-species interactions would be the dominant influence on microbiome membership and the source and target would become less similar over time.

To calculate connectivity strength using aqueous geochemistry (σ_g), we first normalized ion concentrations by their mean and standard deviations and conducted a principle component analysis (PCA) on all major ions present including sodium, chloride, calcium, magnesium, potassium and sulfate ions. Analytical results included several outlying values for chloride and potassium that were removed due to suspected contamination. To maintain a balanced dataset, we replaced the removed outliers by linearly interpolating reported values from the previous and subsequent weeks at the same site. We examined PCA eigenvalues and eigenvectors (Figure 1, Table S1), and based on variable loadings chose to include two principle components (PCs) for further analysis that represented two major water source components. At each sampling date, within the 2-dimensional PC space (PC1 and PC2), the log transformed Euclidean distance was calculated between a given target site geochemical composition and the geochemical composition at Inflow (i.e., source site) (Eq. 2). This value was then rescaled to between 0 and 1 using a min-max normalization and reversed to calculate a chemical similarity score as follows (Eqs. 1 & 2).

$$ED_i = log\left(\sqrt{(PC1_{s_i} - PC1_{t_i})^2 + (PC2_{s_i} - PC2_{t_i})^2}\right) \quad \text{(Eq. 1)}$$

$$\sigma_i = 1 - \left(\frac{ED_i - \min(ED)}{\max(ED) - \min(ED)}\right) \quad \text{(Eq. 2)}$$

Where ED_i is the logged Euclidian distance within the PCA space on a given sampling date, the subscripts s_i and t_i refer respectively to PC scores at Inflow (i.e., the source) and a target site, σ_i is the connectivity strength on a given sampling date and ED is the complete dataset.

To calculate connectivity strength using microbiome membership (σ_m), on each sample date, we calculated a similarity score using the Bray-Curtis similarity index (BC) between microbiome membership at a given target site and Inflow (i.e., the source), as follows (Eq. 3).

$$BC_{st} = \frac{2C_{st}}{S_s + S_t} \qquad \text{(Eq. 3)}$$

Where C is the sum of the lower of the two counts of each OTU found at both sites while S_s is the total number of sequence reads at Inflow and S_t is the total number of sequence reads at the target site. We also conducted a principle coordinate analysis (PCOA) using the BC dissimilarity index to visualize microbiome membership in lower dimensional space (Figure 1c).

To identify the relationship between Inflow stage and site-level connectivity, at each site, we fit natural cubic spline regression equations between Inflow stage and connectivity strength for both geochemical and microbial metrics using the *splines* package in R (R Core Team, 2016). As with relative stage (i.e., stage z-scores), because hysteresis was observed at two sites, we only used the peak through recession period for the model fitting procedure. At Inflow stages that were outside the range of values when connectivity strength was measured in the field (at very high or very low stages), we assigned a constant value for connectivity strength equal to the mean of measured connectivity strength values measured at the four sampling dates with either the highest or lowest Inflow stage. Using these models, we then generated daily time series of connectivity strength at each site using the Inflow stage record for 2018.

2.5 Metric Evaluation

We evaluated the use of geochemical (σ_g) and microbial (σ_m) connectivity strength metrics using several approaches. First, we compared σ_g and σ_m against the conservative tracer (NaCl) injection results including a binary assessment of arrival or no response of the injected tracer. At sites with arrival, we calculated Pearson correlation coefficients between σ_g and σ_m and time to peak of the tracer breakthrough curve (i.e., advective time). To compare connectivity strength metrics against the relative

stage dataset, we calculated durations of connectivity between source and each target site. For relative stage, connectivity duration was defined as the percent of the study period when Inflow stage was above the determined inflection point in source-target stage relationships as described in section 2.4. For σ_g and σ_m, connectivity duration was defined as the percent of the study period in which σ_g and σ_m were above 0.5. Pearson correlation coefficients were calculated to compare whether metrics performed similarly across all sites. To explore the sensitivity of results to a chosen connectivity strength threshold, we also calculated the daily number of connected sites using thresholds ranging from the 10^{th} to 90^{th} percentile of σ_m (0.24 to 0.79).

2.6 Multiple Year Comparison

To compare connectivity dynamics across multiple years, we made use of five years of seasonally monitored water levels (May through September) at Inflow, starting in 2016 through 2020. These stage records were collected with TruTrack Capacitance Rods and were summarized to mean daily stage. As several data gaps in the record exist, we imputed gaps using spline regressions with daily streamflow records from a nearby USGS gage at the Big Thompson River below Moraine Park, Colorado (USGS #402114105350101) (Figure S5). As seasonal hysteresis was observed in the relationship between the North St. Vrain and Big Thompson rivers, spline regression equations were fit separately for the rising limb and falling limb, which were respectively defined as prior and post peak seasonal flow at the North St Vrain.

From this five year record of Inflow stage, we used the connectivity strength models developed for each target site within the 2018 study period (described above) to predict daily connectivity strength values at each target site across all five years from 2016 to 2020 between May 01 and September 30th. To examine how much inter-annual variability was observed at target sites within the river-floodplain system, we calculated the duration of high connectivity ($\sigma_m \geq 0.6$), intermediate connectivity ($0.4 < \sigma_m < 0.6$), and low connectivity ($\sigma_m \leq 0.4$) at each target site for each year. Intermediate connectivity was chosen as between $0.4 < \sigma_m < 0.6$ because analysis of the connectivity strength functions suggest that at low connectivity σ_m stabilized between 0.2 to 0.4, and at high connectivity between 0.6 and 0.8. To examine the effects of inter-annual streamflow variability across the river-floodplain system, we calculated

311 the daily fraction of target sites with high, intermediate and low connectivity. Only the seven target sites
312 with observed intermittent connectivity in 2018 were included in this portion of our analysis.

313 All analyses and related figures were generated in R version 3.6.1 (R Core Team, 2016).

314 **3. Results**

315 *3.1 Hydrometric Monitoring and Tracer Experiment:*

316 Stream levels in the North St Vrain River followed a seasonal pattern consistent with snow driven
317 hydrographs of the Southern Rockies with rising streamflow starting in late April, peak flows in late May to
318 early June and falling streamflow throughout the late-summer/early-fall months (June – September)
319 (Figure 1a). Several summer convective storm events occurred in July and August but did not strongly
320 influence the seasonal hydrograph (Figure 1a). Using stage and geochemical patterns at Inflow (Figure
321 1a), we categorized four distinct hydro-periods: (I) rising limb (May 01, 2018 – May 15, 2018); (II) peak
322 flow (May 16, 2018 – June 18, 2018); (III) falling limb (June 19, 2018 – July 10, 2018); and (IV) recession
323 (July 11, 2018 – Sept 30, 2018) (Figure 1).

324 Analysis of patterns between Inflow stage and relative stage (i.e., stage z-scores) at target sites
325 indicated that target sites generally followed the broad seasonal pattern of streamflow at Inflow but also
326 demonstrated distinct site-specific behavior (Figures 2 & 3). We used inflection points in source-target
327 stage relationships to infer changes or thresholds in hydrologic connectivity between Inflow and floodplain
328 sites. The stage at which inflection points (I_{stage}) in source-target stage relationships occurred varied
329 between sites and spanned a range of Inflow stages from 366 to 642 mm (Figures 2 & 3, Table S1). At
330 the major channel sites, relative stage was strongly coherent with Inflow stage throughout the study
331 period and inflection points in the source-target stage relationship represented only small changes in
332 slope (0.001- 0.004, see Figure 2). At Outflow, the inflection point occurred at very high flow (I_{stage}: 642
333 mm) and the slope change was very low (0.001) suggesting the potential for a false positive, possibly
334 driven by a shift at the site to overbank flooding.

335 At side channel sites, relative stage generally followed patterns similar to Inflow stage with the
336 exception of Side-01 that exhibited hysteretic behavior with higher stage relative to the Inflow during the

337 rising limb compared to the falling limb and recession (Figure 3: panels Side-01, -02, -03 and -04).
338 Inflection points were identified across a wide range of streamflows ranging from the lowest at Side-02
339 (I_{stage}: 366 mm) to the highest at Side-03 (I_{stage}: 597 mm).

340 Both of the surface connected ponds (Pond-Con-01 & Pond-Con-02) and the isolated pond (Pond-
341 Iso) had high water levels starting in the rising limb that did not fluctuate strongly as a function of Inflow
342 stage (slopes 0.001 to 0.003). At all three ponds, water levels declined rapidly relative to Inflow stage
343 below the inflection point (see Figure 3). The inflection point occurred during the falling limb at Pond-Con-
344 02 (I_{stage}: 621 mm), and at much lower flows during the recession at Pond-Con-01 (I_{stage}: 368 mm) and
345 Pond-Iso (I_{stage}: 398 mm) (Figure 2). Like Side-01, Pond-Con-02 exhibited hysteretic behavior with higher
346 stage relative to the Inflow on the rising limbs than on the falling limb. The high water levels in pond sites
347 during the rising limb suggest sampling began after ponds had mostly filled with groundwater, local
348 snowmelt, and streamwater. Pond-Con-01 and Pond-Con-02 went dry in mid-September while at Pond-
349 Iso, levels dropped below our water level logger in early September and the pond went completely dry in
350 late September (Figure 3).

351 The hysteretic behavior observed at Side-01 and Pond-Con-02, which are connected to each other by
352 a surface channel (Figure 1b), may be related to a failure of a beaver dam during peak flows. While we
353 did not identify the specific failed dam, such failures are common in beaver impacted systems and
354 change the thresholds in river stage at which floodplain features have surface connections (Westbrook et
355 al., 2011).

356 The tracer injection experiments conducted during high (June 13, 2018, Inflow stage: 635 mm) and
357 low flows (July 30, 2018, Inflow stage: 384 mm) demonstrated the presence or absence of surface water
358 connectivity between Inflow and a subset of target sites (Table 1). While tracers can also move through
359 sub-surface flowpaths, the instantaneous tracer injection cannot detect flowpaths with very long residence
360 times, and as such tracer arrival primarily reflects surface connectivity within our system. We did not
361 observe arrival of injected tracer at Pond-Iso during either experiment, providing evidence of a lack of
362 strong surface connectivity between Inflow and this site (Table 1). Tracer arrivals at other sites were
363 variable, and we only observed tracer arrival during both the high and low flow injections at the Major

Channel sites (Table 1). During the high flow tracer injection, tracer arrival was first observed at Main-Mid with a time to peak (TTP) of 22.5 minutes, followed by Side-01 (TTP: 35 min), Outflow (TTP: 46 min) and a more delayed arrival at Pond-Con-02 (TTP: 101 min) and Pond-Con-01 (TTP: 196 min) (Table 1). Modal velocity, which is defined as the most common velocity along a flowpath, was highly variable at connected sites (range: 0.09 - 0.87 m s^{-1}, Table 1) indicating variable residence times along connected flow pathways. During the low flow tracer, the tracer arrival was only observed at the Main-Mid site (TTP: 40.8 min, $Vel_{m:}$ 0.48 m s^{-1}) and Outflow site (TTP: 85 min, $Vel_{m:}$ 0.43 m s^{-1}). Given the limits of detecting tracers at high residence times noted above, the lack of response at Side-01, Pond-Con-01 and Pon-Con-02 during the low flow injection cannot confirm a complete absence of surface connectivity. However, these results demonstrate that during the low flow experiment, Side-01, Pond-Con-01 and Pon-Con-02 were not strongly connected with the Inflow site.

3.2 Seasonal Dynamics in Aqueous Geochemistry and Microbiome Membership

Using a principal component analysis, we identified which geochemical indicators were most representative of connectivity and generated a reduced dimensional space with uncorrelated components. The primary principal component (PC1) corresponded to bulk ionic strength and explained 62.2% of the variance in water chemistry and the secondary principal component (PC2) explained 17.8% of variance and was strongly driven by SO_4^{2-} concentrations (Figure 1c, Table S2). All ion concentrations were negatively related to PC1 with Na^+, Ca^{2+}, Cl^-, Mg^{2+}, and K^+ having moderate loadings (between -0.39 to -0.48). SO_4^{2-} had a strong positive loading on PC2 (0.84) while $Ca^{2+}$and Mg^2 had moderate negative loadings (-0.36 and -0.30, respectively).

Seasonal geochemical patterns at Inflow followed a snowmelt dilution pattern where geochemical ion concentrations (e.g., Na^+) were lowest during peak flows (Figure 1, S1 & S2). This geochemical pattern propagated strongly to sites with surface connections to the river during high flows resulting in high geochemical connectivity strength (σ_g) (Figures 2 & 3). As stage declined, geochemical composition diverged between Inflow and most floodplain target sites, resulting in lower σ_g values (Figure 2 & 3). Floodplain target sites crossed the 0.5 σ_g value across a wide range of Inflow stages (I_{geo}) from 351 to 650 mm, demonstrating substantial heterogeneity in connectivity dynamics across the river-floodplain

system. Connectivity strength at Main-Mid and Outflow never declined below 0.5 while Pond-Iso had distinct geochemistry from Inflow throughout the season resulting in low σ_g across the study period that never exceeded 0.5. A sharp decline in σ_g at Pond-Iso was observed at low Inflow stages during the period that the pond was going dry, which may be the result of evapo-concentration (Figure 3),

Using a principal coordinates analysis (PCOA), we explored seasonal dynamics in microbiome membership and examined the potential to utilize microbiome membership as an indicator of connectivity. The PCOA of microbiome membership identified a major axis PCOA-1 that explained 32.5% of the variance in microbiome membership and a secondary axis that explained 15.9% of the variance (Figure 1c). All additional axes explained less than 10% of the variance. Microbial membership at Inflow was relatively stable between the rising limb and falling limb, with more observable shifts in membership at Inflow observed during the recession period (Figure 1c, S3 & S4). During peak flows, sites with structural surface connections to the river had microbiomes similar to Inflow, resulting in high microbial connectivity strength (σ_m) values (Figure 2 & 3). Major channel sites maintained their similarity to Inflow for most of the study period with some divergence at the lowest flows later in hydrograph recession. At side channels and connected pond sites, microbiome membership started diverging from the seasonal pattern at Inflow in either the falling limb or recession hydro-period, resulting in lower σ_m values later in the season (Figure 2 & 3). Floodplain target sites crossed the 0.5 σ_m value at Inflow stages (I_{micro}) ranging from 308 to 577 mm. Like with the geochemical metric, the model fit for σ_m at Main-Mid and Outflow never declined below 0.5 while Pond-Iso had distinct microbial membership from Inflow throughout the season with low σ_m across the study period that never exceeded 0.5.

3.3 Comparison of Connectivity Metrics

Both geochemical and microbial connectivity strength metrics performed well in discriminating between sites that were connected as determined by tracer injections compared to sites where we did not observe arrival of injected tracer (Table 1, Figure 4). Across both injections, sites with observed tracer arrival had higher connectivity strength values (σ_g: =0.67 (mean) ± 0.02 (SE), σ_m: 0.77 ± 0.03) than did sites with no observed tracer arrival (σ_g: 0.33 ± 0.06, σ_m: 0.31 ± 0.03). At sites with observed tracer arrival, σ_m was strongly negatively correlated (R = -0.90, p-value< 0.01) with time to peak (TTP) of the breakthrough

418 curve, while σ_g was only moderately negatively correlated with TTP (R = -0.59, p-value= 0.16) suggesting
419 σ_m may be more responsive to residence time than σ_g. Because Pond-Con-01 had high leverage in the
420 correlation analysis, we also ran the analysis without Pond-Con-01 and found that σ_m was still negatively
421 correlated with TTP (R = -0.74, p-value = 0.09), however there was no longer any correlation between σ_g
422 and TTP (R=-0.03, p-value=0.96).

423 In comparing the connectivity duration above 0.5 (C_{dur}) for each site, σ_m and σ_g generated similar
424 results across sites (R = 0.96) but both generated substantially different results than the C_{dur} as measured
425 with relative stage (σ_m: R = -0.13; σ_g: R = -0.13) (Figure 5a & 5b). Both σ_m and σ_g metrics identified stable
426 connected conditions (100% C_{dur}) at Main-Mid and Outflow and stable disconnected conditions at Pond-
427 Iso (0% C_{dur}, Figure 5c). Conversely, the source-target stage relationship analysis identified connectivity
428 inflection points at Outflow, Pond-Iso, and Main-Mid with C_{dur} ranging from low at Outflow (17% C_{dur}) and
429 moderate at Pond-Iso (55% C_{dur}) and Main Mid (61% C_{dur}, see Figure 5a & b). Even without these three
430 sites, C_{dur} as derived from source-target stage relationships was poorly correlated with C_{dur} as assessed
431 with σ_m (R = 0.21) and σ_g (R = 0.24, see Figure 5). Despite strong correlations between C_{dur} derived from
432 σ_m and σ_g, there were several sites with substantively different C_{dur} between metrics including Pond-Con-
433 01 (σ_m = 46%, σ_g = 63%), Main-Braid (σ_m = 80%, σ_g = 64%) and Side-04 (σ_m = 30%, σ_g = 15%).

434 *3.4 Connectivity Regimes*

435 Across the 2018 study period, sites identified as stable (C_{dur} = 0% or 100%; Outflow, Main-Mid, & Pond-
436 Iso) had generally unimodal distributions of connectivity strength with modes at high or low values (Figure
437 6). In contrast, distributions of connectivity strength at the remaining seven sites with intermittent
438 connectivity, had wide spread and a dominant mode at lower connectivity values and a secondary mode
439 at high connectivity values (Figure 6). Within the intermittent target sites, some sites such as Side-03 and
440 Pond-Con-02 exhibited rapid shifts between modes with few observed sample dates with intermediate
441 connectivity strength while others including Pond-Con-01, Side-01, and Side-02 exhibited more gradual
442 behavior with intermediate connectivity strength values for a larger proportion of the study period (Figures
443 3 & 6).

Aggregating site specific results to the river-floodplain system reveals transitions in system connectivity. At high flows, conditions are more homogenous and there is relatively high connectivity across the entire river-floodplain system (Figure 7a & b). Conversely, there was a bimodal distribution of river-floodplain connectivity at lower flows with some sites remaining connected and others becoming disconnected from Inflow. The mean value of σ_m across the river-floodplain system was positively related to Inflow stage (Figure 7c), whereas the variance in connectivity, as derived from the standard deviation of σ_m, was highest during intermediate flows (Figure 7d).

At the river-floodplain system scale, we also found that defining binary σ_m connectivity thresholds to describe the system wide behavior can be sensitive to the chosen σ_m threshold value (Figure 8). We varied the threshold between the 10th to 90th percentiles of σ_m and observed the effect on exceedance probabilities of how many sites are connected in the 2018 study period. Varying σ_m thresholds between 0.4 to 0.6 generated small shifts in the exceedance probabilities distributions. Outside that range, exceedance probability distributions exhibited larger changes in their shape (Figure 8).

3.5 Inter-Annual Variability in Floodplain Connectivity

Our modeled river-floodplain system connectivity dynamics differed across years reflecting the influence of inter-annual variability in the timing and magnitude of seasonal snowmelt hydrographs (Figure 9). To measure the inter-annual variability (henceforth called total sensitivity), at each intermittently connected target site we calculated the difference between years with the highest and lowest values of duration (% of period) within three connectivity states: high ($\sigma_m > 0.6$), intermediate ($0.4 < \sigma_m > 0.6$) and low connectivity ($\sigma_m < 0.4$) (Table 2). Total sensitivity ranged between 16 to 22% for duration of high connectivity, 6 to 16% for intermediate connectivity, and 10 to 25% for low connectivity (Figure 9a). Along with generally lower total sensitivity for intermediate connectivity, the duration that sites spent in intermediate connectivity was also low, with intermediate connectivity duration ranging between 5% to 26% of the study period across all intermittently connected target sites and years (Table 2, Figure 9a). This sensitivity is also reflected in the exceedance probabilities (% of period) of the percent of intermittent sites in high, intermediate and low connectivity states. As one would expect, in wetter years, intermittent

sites remained in a high connectivity state for longer, while in dry years these sites had longer durations in low connectivity states (Figure 9b).

4. Discussion

Coupling hydrometric measurements such as stage with estimates of geochemical and microbial connectivity strength is useful for describing spatiotemporal patterns in connectivity at both target site specific and river-floodplain system scales. At the target site specific level, source-target stage relationships reveal patterns of hydrologic response to both shifting river flows and subsurface groundwater levels. While high water levels are associated with higher connectivity, source-target stage relationships are sensitive to both shifts in connectivity type and the site-level geomorphic controls on water level. However, these relationships do not necessarily contain information about the type of connectivity present (surface vs subsurface) without additional contextual information. For example, in our study both Pond-Con-01 and Pond-Iso demonstrated similar source-target stage relationships with Inflow throughout the hydrograph even though Pond-Iso likely had little to no surface connection with Inflow, whereas Pond-Con-01 did have surface connectivity. As such, source-target stage relationships did not reveal differences in surface connectivity between Pond-Con-01 or Pond-Iso and Inflow. However, our connectivity metrics derived from geochemical (σ_g) and microbial (σ_m) indicators did identify differences in connectivity between Pond-Con-01 and Pond-Iso and Inflow. Specifically, both σ_g and σ_m revealed low connectivity between Inflow and Pond-Iso but higher connectivity strength values between Inflow and Pond-Con-01 during high flows, both of which match our visual field observations of surface water connections. Accordingly, source-target stage relationships alone did not provide insight to functional connectivity defined by the observed influence of the source site on the target site, whereas geochemical and microbial indicators did. Therefore, we focus on the σ_g and σ_m connectivity strength metrics to describe spatial and temporal patterns of connectivity within the river-floodplain system.

4.1 Connectivity Strength as a Continuous Measure

Treating connectivity as a continuous value measured with geochemical and microbial metrics successfully enabled the development of target site specific connectivity functions that described site

497 specific behavior in response to fluctuations in stage at Inflow. Our evaluation of the geochemical and
498 microbial connectivity strength metrics confirmed that both performed well in distinguishing between
499 target sites with high and low connectivity as identified by where tracer breakthrough curves were
500 observed during experimental tracer injections (Figure 4). The site specific connectivity functions allowed
501 us to predict connectivity at each target site daily throughout the main study period (May 01, 2018 through
502 September 01, 2018) and subsequently predict connectivity behavior from previous years (2016 through
503 2020) using only information from the Inflow stage measurements.

504 Using daily connectivity predictions for the 2018 study period, we identified three major surface water
505 connectivity regimes operating within the river-floodplain system during the study period (Figure 6). Sites
506 were observed to have: high σ_m values and low spread for the majority of the study period, low σ_m values
507 and spread, or intermittently connected with a wide range of σ_m values that varied with Inflow stage
508 (Figures 5 & 6). The sites that had high σ_m for a large proportion of the study period were those located
509 along the main stem of the river. Interestingly, these sites also exhibited evidence of a shift toward
510 decreased σ_m at very low streamflows (Figures 2 & 5), perhaps reflecting increased transit time or
511 alternatively, changes in source water composition within the reach. The only site to demonstrate low σ_m
512 values throughout the study was Pond-Iso where we observed no surface connection to the main channel
513 and which had a unimodal distribution of low σ_m values despite being geographically near Inflow (Figure
514 1b), demonstrating that geographic proximity does not dictate high hydrologic connectivity. At sites with
515 intermittent connectivity regimes, interactions between river flow dynamics and floodplain geomorphic
516 structures generated target site-specific variability in connectivity regimes. Distributions of connectivity
517 strength at all intermittent sites, except at Main-Braid, were characterized by a dominant mode of low
518 connectivity strength and a secondary mode of higher connectivity strength (Figure 6). This reflects that at
519 the majority of floodplain target sites, high connectivity values are only maintained at Inflow stages well
520 above the median stage of 424 mm during the 2018 study period.

521 While this bimodality at intermittently connected target sites makes a case for treating connectivity as
522 binary, evaluation of site specific data also indicated that some sites experience prolonged periods of
523 intermediate connectivity strength. If we consider σ values of $0.4 < \sigma < 0.6$ to be intermediate

connectivity, then during the 2018 study period, sites spent as little as 7% and as much as 33% in a state of intermediate connectivity (ranges: $\sigma_{m:}$ 7%-20%; $\sigma_{g:}$ 10-33%). Identifying places with longer durations of intermediate connectivity is thought to be particularly important for identifying control points in a landscape that have disproportionate influence on hydrologic and biogeochemical properties of the ecosystem (Bernhardt et al., 2017). In river-floodplain systems, sites with high durations of intermediate connectivity may act as such because they can have a substantial flux of river water moving through them but also long enough residence times for biogeochemical processes that are distinct from those in the main stem river to occur (Covino, 2017; Lynch et al., 2019).

4.1.1 Microbiomes as complementary sources of connectivity information

While geochemistry and microbiome membership were broadly similar when calculating connectivity metrics such as connectivity duration (Figure 5), we also observed key distinctions that illustrate how microbiome membership may provide additional information about connectivity not observed in hydrologic and geochemical metrics. Within our system, σ_m was strongly negatively correlated with time to peak during our tracer experiments suggesting that σ_m is responsive to residence times (Figure 4). In contrast, σ_g was less well correlated with time to peak (Figure 4). This is consistent with known differences in drivers between the two metrics. Geochemistry will reflect mixing of source waters which may or may not be related to residence times. In contrast, ecological theory states that microbial communities are shaped not just by dispersal but also by local ecological dynamics that come to dominate microbiome assembly as residence time becomes greater than growth rate (Lindström et al., 2005). As flow decreases and residence times increase in a water body, selection driven by local environmental conditions is likely to become a larger factor relative to dispersal (i.e., immigration and emigration) in determining microbiome membership (Mayr et al., 2020), which could result in increasing dissimilarity in microbiome membership between a source and target location.

This shift towards a selection driven microbial community assembly may be most observable when residence times increase above a certain threshold, which might help explain the differences we observed at Pond-Con-01 between the microbial and geochemical connectivity metrics (Figure 3 & 5, Table S1). At Pond-Con-01, σ_m had a gradual, mostly linear relationship with Inflow stage with an

551 inflection point at moderate Inflow stage (I_{micro}: 456 mm, see Figure 3), while pond stage remained high at
552 these flows. In contrast, σ_g was relatively invariant with Inflow stage until a sudden drop at low Inflow
553 stage (I_{geo}: 360 mm), which occurred at nearly the same Inflow threshold (I_{stage} = 368 mm) that stage in
554 the pond began falling (Figure 3). The surface flowpath between the river and Pond-Con-01 passed
555 through several beaver ponds before reaching the site. As a result, even at peak river flows, water
556 velocities through Pond-Con-01 were low, and travel times were long, relative to other sites (Table 1). As
557 streamflow declined, the water flux into the pond also decreased and residence times increased because
558 pond levels and volume remained stable. Through this period, the stable levels and persistence of high
559 geochemical connectivity strength suggest a surface flow connection to the river was maintained, but the
560 degree of influence of the river on the pond microbiome declined. Thus, from a functional connectivity
561 perspective, one could either say the site was at different connectivity strengths with the Inflow depending
562 on which metric was examined. This reinforces that functional connectivity is defined by the metric of
563 interest and interpretation requires considering what aspects of connectivity are being reflected by each
564 measurement approach (Wohl et al., 2019).

565 *4.2 Connectivity Regimes: Scaling from Site to System Scales*

566 Aggregating target site specific dynamics to river-floodplain system scale behavior is critical for
567 understanding how river connectivity in floodplains impacts broader landscapes processes. While our
568 analyses here are limited due to our relatively small sample size of sites, aggregation of site behavior did
569 reveal important distinctions between mean system behavior and spatially distributed behavior. As
570 conceptualized in the flood and flow pulse concepts (Junk et al., 1989; Tockner et al., 2000), mean
571 connectivity across the river-floodplain system rose as streamflow increased (Figure 7c). Thus, while
572 threshold-like behavior was observed at many individual sites, mean system behavior followed a
573 continuous gradient because the connectivity thresholds were highly variable among sites. However, it is
574 also clear that the mean is a poor descriptor of the spatially aggregated behavior, particularly at lower
575 river flows when connectivity strength values across the floodplain had a bimodal distribution with some
576 sites maintaining relatively high connectivity while the majority were disconnected. This has important
577 implications for scaling many spatially distributed biogeochemical and ecologic processes impacted by

connectivity such as carbon production and storage, nutrient retention, and methane fluxes (Lynch et al., 2019; Roley et al., 2012; Samaritani et al., 2011; Sutfin et al., 2016).

Aggregating site-specific behavior also demonstrated that river-floodplain system-wide variance in connectivity was maximized at intermediate river flows. The low variance in connectivity observed at high river flows (Figure 7c) is consistent with the flood homogenization theory that physical and chemical states across floodplains are more similar at high flows (Thomaz et al., 2007). Our results also support the idea that physio-chemical condition at individual sites in floodplains are most different from the river at the lowest flows (low σ values) due to isolation. However, our findings diverge from the homogenization theory in that peak variability in connectivity dynamics was observed at intermediate flows rather than low flows as the theory suggests. Thus, while individual sites might be most different from each other at lowest flows due to isolation, the distribution of connectivity dynamics across the floodplain was most variable when river stage was intermediate and some sites were isolated while others remained strongly or moderately connected to the source.

4.3 *Inter-annual Variability in Connectivity at Site-Specific and River-Floodplain System Scales*

In watersheds characterized by a single large snowmelt event, hydrologic variability is often driven by inter-annual variation in snowpack accumulation and melting that regulates the timing and magnitude of streamflow (Hammond et al., 2018). In floodplains within these watersheds, whether connectivity regimes are sensitive to this inter-annual variability will depend on the interactions between streamflow hydrographs and the physical structure of river-floodplain connections and corresponding thresholds. As future climate predictions indicate lower snowpack, earlier snowmelt and drier late season conditions (Barnett et al., 2005; Stewart et al., 2005), assessing the degree of sensitivity is important for understanding how future hydro-climatic regimes may change connectivity in river-floodplain systems. Our connectivity predictions for five years at intermittent sites highlight that site-specific and river-floodplain system scale connectivity regimes are sensitive to streamflow variability with substantial year to year shifts in the duration of high and low connectivity. However, within a given river-floodplain system, there will be spatial variation in sensitivity that will be driven by the river-floodplain physical structure and corresponding stage thresholds, but also by the manner of changes in streamflow hydrographs. This can

observed in our dataset by comparing floodplain connectivity in two low flow years: 2018 and 2020. In 2018, we observed the lowest peak flows at Inflow in the five year dataset but 2018 had a longer duration of medium to high flows than was observed in 2020 (Figures 8 & S5). As a result, a majority of sites remained highly connected for longer in 2018 than 2020, while durations of intermediate connectivity were highest in 2020. As such, efforts to understand how climate change will alter floodplain function in snowmelt watersheds will need to consider both changes to flow magnitudes and to flow durations generated by changing climatic conditions.

4.4 Limitations and Recommendations for Future Research

While the approach developed in this manuscript successfully describes spatiotemporal connectivity dynamics, there are several assumptions and limitations that future work should consider. Connectivity strength metrics used here enable the development of a continuous value between 0 and 1, however the meaning of the connectivity strength values are dependent on the internal variation within a system and interpretation may differ among systems. As such, we suggest that when identifying thresholds in different connectivity states, future research should consider a distribution of possible connectivity strength values (see Figure 9). An additional limitation is that the empirical connectivity functions we developed assume stationarity in the underlying floodplain structure and fitting a single model assumes a lack of hysteresis in functional connectivity between source and target sites between rising and falling limbs. Our observations of hysteresis at two sites in 2018, likely driven by beaver activity, suggests that such changes in connectivity thresholds are likely relatively common. However, such assumptions are equally present in all approaches reliant on static physical datasets such single date LIDAR acquisition or field surveys (Passalacqua et al., 2015). Therefore, we believe our approach is valuable but for longer-term studies, but that conditions should be monitored through time and relationships updated similar to how a rating curve used to estimate discharge needs to be updated if the underlying channel morphology is altered during the study period.

While our work demonstrates that aquatic microbiomes can be utilized for inference into hydrologic connectivity, our ability to determine the broad applicability of this technique is limited. This study was conducted in a relatively small river-floodplain system with relatively homogenous surrounding land cover.

To apply the microbial connectivity metric more widely, future work will need to assess how residence time thresholds in different systems and at different scales interact with microbial membership. Further, as investigations move to larger, more heterogeneous landscape scales, it will be necessary to consider how to incorporate more diverse sources of water and microbiomes into the approach. To address this, we suggest that future work implement finer-scale OTU-level analysis rather than a coarse community level similarity metric, which we believe can increase the ability to detect weaker flow paths and potentially be used as a multi-tracer to simultaneously measure connectivity from multiple water sources.

5. Summary

In this study, we developed and applied an approach to assess the strength of hydrologic connections between a source and target sites within a river-floodplain system using field-based indicators. We defined the source as the river at the upstream boundary of the river-floodplain system with target sites both downstream within the river channel and laterally distributed across the floodplain. Using a field-based dataset, we generated empirical models to describe target site-specific connectivity strength as a function of source stage, and then predicted daily connectivity strength for five years between May and September of 2016 through 2020. Within this approach we also tested the use of aquatic microbiomes as a metric of hydrologic connectivity. By examining similarity in microbial membership, we accurately assessed the presences/absences of surface flows from the source to target sites and found that aquatic microbiomes can provide additional information on residence time dynamics along connected surface flow paths.

Our results demonstrate that connectivity in aquatic water bodies in the river-floodplain system can either be stable or intermittent. Intermittently connected target sites can differ widely in source connection/disconnection thresholds. While some target sites demonstrate binary connectivity behavior quickly changing between high and low connectivity states, others display gradual behavior with substantial durations at intermediate connectivity levels. When aggregated to the river-floodplain system scale, mean system-scale connectivity increased with stage due to the influence of averaging across sites with heterogeneous conditions. However, we demonstrate that mean behavior is a poor descriptor of

river-floodplain system behavior because spatial distributions of connectivity across all sites tend toward bimodality at intermediate and lower flows, reflecting conditions when river stage is sufficient to enable connectivity for only a portion of the system. As a result, the spatial heterogeneity of connectivity state peaked at intermediate river stage values. We also demonstrate that connectivity regimes are sensitive to inter-annual variation in streamflow and that while differences in the magnitude of peak flow are important so are changes to the flow duration across the range of differing flow states. Therefore, predictions of how river-floodplain connectivity will change due to climate change and/or other disturbances to hydrologic regimes need to consider the impacts across the full range of potential flows.

5. Acknowledgements

We thank Connor Lockwood and Chris Sunblade for field assistance and Tim Fegel and Kristen Otto for lab assistance, and Rocky Mountain National Park for site access and the Rocky Mountain Research Station for use of their lab facilities. This material is based on work suppported by the National Science Foundation EAR grant numbers 1632798 and 1945504, Department of Energy SBR grant number 0000241776, and a NASA National Earth and Space Science Fellowship awarded to Alex Brooks. Data and relevant scripts are publically available on CUAHSI Hydroshare Repository and will be published at http://www.hydroshare.org/resource/4f7167faa71746be987b74bb227e83b8.

676 Addy, S., & Wilkinson, M. E. (2019). Representing natural and artificial in-channel large wood in numerical
677 hydraulic and hydrological models. *WIREs Water*, *6*(6), 1–20. https://doi.org/10.1002/wat2.1389

678 Amalfitano, S., Del Bon, A., Zoppini, A., Ghergo, S., Fazi, S., Parrone, D., … Preziosi, E. (2014).
679 Groundwater geochemistry and microbial community structure in the aquifer transition from volcanic
680 to alluvial areas. *Water Research*, *65*, 384–394. https://doi.org/10.1016/j.watres.2014.08.004

681 Amoros, C., & Bornette, G. (2002). Connectivity and biocomplexity in waterbodies of riverine floodplains.
682 *Freshwater Biology*, *47*(4), 761–776. https://doi.org/10.1046/j.1365-2427.2002.00905.x

683 Apprill, A., McNally, S., Parsons, R., & Weber, L. (2015). Minor revision to V4 region SSU rRNA 806R
684 gene primer greatly increases detection of SAR11 bacterioplankton . *Aquatic Microbial Ecology*,
685 *75*(2), 129–137. Retrieved from https://www.int-res.com/abstracts/ame/v75/n2/p129-137/

686 Barnett, T. P., Adam, J. C., & Lettenmaier, D. P. (2005). Potential impacts of a warming climate on water
687 availability in snow-dominated regions. *Nature*, *438*(7066), 303–309.
688 https://doi.org/10.1038/nature04141

689 Bellmore, J. R., & Baxter, C. V. (2014). EFFECTS OF GEOMORPHIC PROCESS DOMAINS ON RIVER
690 ECOSYSTEMS: A COMPARISON OF FLOODPLAIN AND CONFINED VALLEY SEGMENTS. *River*
691 *Research and Applications*, *30*(5), 617–630. https://doi.org/10.1002/rra.2672

692 Bernhardt, E. S., Blaszczak, J. R., Ficken, C. D., Fork, M. L., Kaiser, K. E., & Seybold, E. C. (2017).
693 Control Points in Ecosystems: Moving Beyond the Hot Spot Hot Moment Concept. *Ecosystems*.
694 https://doi.org/10.1007/s10021-016-0103-y

695 Bracken, L. J., & Croke, J. (2007). The concept of hydrological connectivity and its contribution to
696 understanding runoff-dominated geomorphic systems. *Hydrological Processes*, *21*(13), 1749–1763.
697 https://doi.org/10.1002/hyp.6313

698 Bracken, L. J., Wainwright, J., Ali, G. A., Tetzlaff, D., Smith, M. W., Reaney, S. M., & Roy, A. G. (2013).
699 Concepts of hydrological connectivity: Research approaches, Pathways and future agendas. *Earth-*
700 *Science Reviews*, *119*, 17–34. https://doi.org/10.1016/j.earscirev.2013.02.001

701 Briggs, M. A., Wang, C., Day-lewis, F. D., Williams, K. H., Dong, W., & Lane, J. W. (2019). Science of the
702 Total Environment Return fl ows from beaver ponds enhance fl oodplain-to-river metals exchange in
703 alluvial mountain catchments. *Science of the Total Environment*, *685*, 357–369.
704 https://doi.org/10.1016/j.scitotenv.2019.05.371

705 Cabezas, A., Garcia, M., Gallardo, B., Gonzalez, E., Gonzalez-Sanchis, M., & Comin, F. A. (2009). The
706 effect of anthropogenic disturbance on the hydrochemical characteristics of riparian wetlands at the
707 Middle Ebro River (NE Spain). *Hydrobiologia*, *617*(1), 101–116. https://doi.org/10.1007/s10750-008-
708 9531-9

709 Cabezas, A., Gonzalez-Sanchís, M., Gallardo, B., & Comín, F. A. (2011). Using continuous surface water
710 level and temperature data to characterize hydrological connectivity in riparian wetlands.
711 *Environmental Monitoring and Assessment*, *183*(1–4), 485–500. https://doi.org/10.1007/s10661-
712 011-1934-9

713 Caporaso, J. G., Lauber, C. L., Walters, W. A., Berg-Lyons, D., Lozupone, C. A., Turnbaugh, P. J., …
714 Knight, R. (2011). Global patterns of 16S rRNA diversity at a depth of millions of sequences per
715 sample. *Proceedings of the National Academy of Sciences*, *108*(Supplement 1), 4516 LP – 4522.
716 https://doi.org/10.1073/pnas.1000080107

717 Chen, X., Chen, L., Stone, M. C., & Acharya, K. (2020). Assessing connectivity between the river channel
718 and floodplains during high flows using hydrodynamic modeling and particle tracking analysis.
719 *Journal of Hydrology*, *583*(July 2019), 124609. https://doi.org/10.1016/j.jhydrol.2020.124609

720 Cheng, F. Y., & Basu, N. B. (2017). Biogeochemical hotspots: Role of small water bodies in landscape
721 nutrient processing. *Water Resources Research*, *53*(6), 5038–5056.

https://doi.org/10.1002/2016WR020102

Cohen, M. J., Creed, I. F., Alexander, L., Basu, N. B., Calhoun, A. J. K., Craft, C., … Walls, S. C. (2016). Do geographically isolated wetlands influence landscape functions? *Proceedings of the National Academy of Sciences of the United States of America*, *113*(8), 1978–1986. https://doi.org/10.1073/pnas.1512650113

Covino, T. (2017). Hydrologic connectivity as a framework for understanding biogeochemical flux through watersheds and along fluvial networks. *Geomorphology*, *277*, 133–144. https://doi.org/10.1016/j.geomorph.2016.09.030

Crump, B. C., & Hobbie, J. E. (2005). Synchrony and seasonality in bacterioplankton communities of two temperate rivers. *Limnology and Oceanography*, *50*(6), 1718–1729. https://doi.org/10.4319/lo.2005.50.6.1718

Crump, B. C., Amaral-zettler, L. A., & Kling, G. W. (2012). Microbial diversity in arctic freshwaters is structured by inoculation of microbes from soils, *6*(9), 1629–1639. https://doi.org/10.1038/ismej.2012.9

Fritz, K. M., Schofield, K. A., Alexander, L. C., McManus, M. G., Golden, H. E., Lane, C. R., … Pollard, A. I. (2018). Physical and Chemical Connectivity of Streams and Riparian Wetlands to Downstream Waters: A Synthesis. *JAWRA Journal of the American Water Resources Association*. https://doi.org/10.1111/1752-1688.12632

Garbin, S., Celegon, E. A., Fanton, P., & Botter, G. (2019). Hydrological controls on river network connectivity. *Royal Society Open Science*, *6*(2). https://doi.org/10.1098/rsos.181428

Good, S. P., Urycki, D. R., & Crump, B. C. (2018). Predicting Hydrologic Function With Aquatic Gene Fragments. *Water Resources Research*, *54*(3), 2424–2435. https://doi.org/10.1002/2017WR021974

Hammond, J. C., Saavedra, F. A., & Kampf, S. K. (2018). How Does Snow Persistence Relate to Annual Streamflow in Mountain Watersheds of the Western U.S. With Wet Maritime and Dry Continental Climates? *Water Resources Research*, *54*(4), 2605–2623. https://doi.org/10.1002/2017WR021899

Jones, C. N., Scott, D. T., Edwards, B. L., & Keim, R. F. (2014). Perirheic mixing and biogeochemical processing in flow-through and backwater floodplain wetlands. *Water Resources Research*, *50*(9), 7394–7405. https://doi.org/10.1002/2014WR015647

Jones, K. L., Poole, G. C., Daniel, S. J. O., Mertes, L. A. K., & Stanford, J. A. (2008). Remote Sensing of Environment Surface hydrology of low-relief landscapes : Assessing surface water fl ow impedance using LIDAR-derived digital elevation models, *112*, 4148–4158. https://doi.org/10.1016/j.rse.2008.01.024

Junk, W., Bayley, P. B., & Sparks, R. E. (1989). The flood pulse concept in river-floodplain-systems. *Canadian Journal of Fisheries and Aquatic Sciences*, *106*(September 2014), 110–127. https://doi.org/10.1371/journal.pone.0028909

Laurel, D., & Wohl, E. (2019). The persistence of beaver-induced geomorphic heterogeneity and organic carbon stock in river corridors. *Earth Surface Processes and Landforms*, *44*(1), 342–353. https://doi.org/10.1002/esp.4486

Leibowitz, S. G., Wigington, P. J., Schofield, K. A., Alexander, L. C., Vanderhoof, M. K., & Golden, H. E. (2018). Connectivity of Streams and Wetlands to Downstream Waters: An Integrated Systems Framework. *Journal of the American Water Resources Association*, *54*(2), 298–322. https://doi.org/10.1111/1752-1688.12631

Lindström, E. S., Forslund, M., Algesten, G., & Bergström, A. K. (2006). External control of bacterial community structure in lakes. *Limnology and Oceanography*, *51*(1 I), 339–342. https://doi.org/10.4319/lo.2006.51.1.0339

767 Lindström, E. S., Kamst-Van Agterveld, M. P., & Zwart, G. (2005). Distribution of typical freshwater
768 bacterial groups is associated with pH, temperature, and lake water retention time. *Applied and*
769 *Environmental Microbiology*, *71*(12), 8201–8206. https://doi.org/10.1128/AEM.71.12.8201-
770 8206.2005

771 Lynch, L. M., Sutfin, N. A., Fegel, T. S., Boot, C. M., Covino, T. P., & Wallenstein, M. D. (2019). River
772 channel connectivity shifts metabolite composition and dissolved organic matter chemistry. *Nature*
773 *Communications*, *10*(1). https://doi.org/10.1038/s41467-019-08406-8

774 Martínez-Carreras, N., Wetzel, C. E., Frentress, J., Ector, L., McDonnell, J. J., Hoffmann, L., & Pfister, L.
775 (2015). Hydrological connectivity inferred from diatom transport through the riparian-stream system.
776 *Hydrology and Earth System Sciences*, *19*(7), 3133–3151. https://doi.org/10.5194/hess-19-3133-
777 2015

778 Mayr, M. J., Besemer, K., Sieczko, A., Demeter, K., & Peduzzi, P. (2020). Bacterial community
779 composition and function along spatiotemporal connectivity gradients in the Danube floodplain
780 (Vienna, Austria). *Aquatic Sciences*, *82*(2). https://doi.org/10.1007/s00027-020-0700-x

781 McMurdie, P. J., & Holmes, S. (2013). phyloseq: An R Package for Reproducible Interactive Analysis and
782 Graphics of Microbiome Census Data. *PLOS ONE*, *8*(4), e61217. Retrieved from
783 https://doi.org/10.1371/journal.pone.0061217

784 Muggeo, V. M. R. (2008). Segmented: an R package to fit regression models with broken-line
785 relationships. *R News*, *8*(1), 20–25.

786 Nemergut, D. R., Schmidt, S. K., Fukami, T., O'Neill, S. P., Bilinski, T. M., Stanish, L. F., … Ferrenberg,
787 S. (2013). Patterns and Processes of Microbial Community Assembly. *Microbiology and Molecular*
788 *Biology Reviews*, *77*(3), 342–356. https://doi.org/10.1128/mmbr.00051-12

789 Opperman, J. J., Luster, R., McKenney, B. A., Roberts, M., & Meadows, A. W. (2010). Ecologically
790 functional floodplains: Connectivity, flow regime, and scale. *Journal of the American Water*
791 *Resources Association*, *46*(2), 211–226. https://doi.org/10.1111/j.1752-1688.2010.00426.x

792 Parada, A. E., Needham, D. M., & Fuhrman, J. A. (2016). Every base matters: assessing small subunit
793 rRNA primers for marine microbiomes with mock communities, time series and global field samples.
794 *Environmental Microbiology*, *18*(5), 1403–1414. https://doi.org/10.1111/1462-2920.13023

795 Passalacqua, P., Belmont, P., Staley, D. M., Simley, J. D., Arrowsmith, J. R., Bode, C. A., … Wheaton, J.
796 M. (2015). Analyzing high resolution topography for advancing the understanding of mass and
797 energy transfer through landscapes: A review. *Earth-Science Reviews*, *148*, 174–193.
798 https://doi.org/10.1016/j.earscirev.2015.05.012

799 Pfister, L., Mcdonnell, J. J., Wrede, S., Matgen, P., & Fenicia, F. (2009). The rivers are alive : on the
800 potential for diatoms as a tracer of water source and hydrological connectivity, *2845*(June), 2841–
801 2845. https://doi.org/10.1002/hyp

802 Poole, G. C. (2002). Fluvial landscape ecology: addressing uniqueness within the river discontinuum.
803 *Freshwater Biology*, *47*(4), 641–660.

804 Quast, C., Pruesse, E., Yilmaz, P., Gerken, J., Schweer, T., Yarza, P., … Glöckner, F. O. (2013). The
805 SILVA ribosomal RNA gene database project: improved data processing and web-based tools.
806 *Nucleic Acids Research*, *41*(Database issue), D590–D596. https://doi.org/10.1093/nar/gks1219

807 R Core Team. (2016). R: A Language and Environment for Statistical Computing. Vienna, Austria.
808 Retrieved from https://www.r-project.org/

809 Rains, M. C., Leibowitz, S. G., Cohen, M. J., Creed, I. F., Golden, H. E., Jawitz, J. W., … Mclaughlin, D.
810 L. (2016). Geographically isolated wetlands are part of the hydrological landscape. *Hydrological*
811 *Processes*, *30*(1), 153–160. https://doi.org/10.1002/hyp.10610

812 Read, D. S., Gweon, H. S., Bowes, M. J., Newbold, L. K., Field, D., Bailey, M. J., & Griffiths, R. I. (2014).
813 Catchment-scale biogeography of riverine bacterioplankton. *The ISME Journal*, *9*(2), 516–526.
814 https://doi.org/10.1038/ismej.2014.166

815 Rinderer, M., Ali, G., & Larsen, L. G. (2018). Assessing structural, functional and effective hydrologic
816 connectivity with brain neuroscience methods: State-of-the-art and research directions. *Earth-*
817 *Science Reviews*, *178*(July 2017), 29–47. https://doi.org/10.1016/j.earscirev.2018.01.009

818 Roley, S. S., Tank, J. L., Stephen, M. L., Johnson, L. T., Beaulieu, J. J., & Witter, J. D. (2012). Floodplain
819 restoration enhances denitrification and reach-scale nitrogen removal in an agricultural stream.
820 *Ecological Applications*, *22*(1), 281–297. https://doi.org/10.1890/11-0381.1

821 Roni, P., Hall, J. E., Drenner, S. M., & Arterburn, D. (2019). Monitoring the effectiveness of floodplain
822 habitat restoration: A review of methods and recommendations for future monitoring. *Wiley*
823 *Interdisciplinary Reviews: Water*, *6*(4), e1355.

824 Samaritani, E., Shrestha, J., Fournier, B., Frossard, E., Gillet, F., Guenat, C., … others. (2011).
825 Heterogeneity of soil carbon pools and fluxes in a channelized and a restored floodplain section
826 (Thur River, Switzerland). *Hydrology and Earth System Sciences*, *15*(6), 1757–1769.

827 Savio, D., Sinclair, L., Ijaz, U. Z., Parajka, J., Reischer, G. H., Stadler, P., … Eiler, A. (2015). Bacterial
828 diversity along a 2600km river continuum. *Environmental Microbiology*, *17*(12), 4994–5007.
829 https://doi.org/10.1111/1462-2920.12886

830 Schloss, P. D., Westcott, S. L., Ryabin, T., Hall, J. R., Hartmann, M., Hollister, E. B., … Weber, C. F.
831 (2009). Introducing mothur: Open-Source, Platform-Independent, Community-Supported Software
832 for Describing and Comparing Microbial Communities. *Applied and Environmental Microbiology*,
833 *75*(23), 7537 LP – 7541. https://doi.org/10.1128/AEM.01541-09

834 Stanford, J. A., & Ward, J. V. (1993). An Ecosystem Perspective of Alluvial Rivers: Connectivity and the
835 Hyporheic Corridor. *Journal of the North American Benthological Society*, *12*(1), 48–60.
836 https://doi.org/10.2307/1467685

837 Stewart, I. T., Cayan, D. R., & Dettinger, M. D. (2005). Changes toward earlier streamflow timing across
838 western North America. *Journal of Climate*, *18*(8), 1136–1155. https://doi.org/10.1175/JCLI3321.1

839 Stone, M. C., Byrne, C. F., & Morrison, R. R. (2017). Evaluating the impacts of hydrologic and
840 geomorphic alterations on floodplain connectivity. *Ecohydrology*, *10*(5), 1–11.
841 https://doi.org/10.1002/eco.1833

842 Sutfin, N. A., Wohl, E. E., & Dwire, K. A. (2016). Banking carbon: A review of organic carbon storage and
843 physical factors influencing retention in floodplains and riparian ecosystems. *Earth Surface*
844 *Processes and Landforms*, *41*(1), 38–60. https://doi.org/10.1002/esp.3857

845 Thomaz, S. M., Bini, L. M., & Bozelli, R. L. (2007). Floods increase similarity among aquatic habitats in
846 river-floodplain systems. *Hydrobiologia*, *579*(1), 1–13. https://doi.org/10.1007/s10750-006-0285-y

847 Thompson, L. R., Sanders, J. G., McDonald, D., Amir, A., Ladau, J., Locey, K. J., … Consortium, T. E. M.
848 P. (2017). A communal catalogue reveals Earth's multiscale microbial diversity. *Nature*, *551*(7681),
849 457–463. https://doi.org/10.1038/nature24621

850 Thoms, M. C., Southwell, M., & McGinness, H. M. (2005). Floodplain-river ecosystems: Fragmentation
851 and water resources development. *Geomorphology*, *71*(1–2), 126–138.
852 https://doi.org/10.1016/j.geomorph.2004.10.011

853 Tockner, K., & Stanford, J. A. (2002). Riverine flood plains: Present state and future trends.
854 *Environmental Conservation*, *29*(3), 308–330. https://doi.org/10.1017/S037689290200022X

855 Tockner, K., Malard, F., & Ward, J. V. (2000). An extension of the flood pulse concept. *Hydrological*
856 *Processes*, *14*(16–17), 2861–2883. https://doi.org/10.1002/1099-

1085(200011/12)14:16/17<2861::AID-HYP124>3.0.CO;2-F

Tockner, K., Malard, F., Uehlinger, U., & Ward, J. V. (2002). Nutrients and organic matter in a glacial river – floodplain system (Val Roseg ,. *Limnology and Oceanography*, *47*(1), 266–277. https://doi.org/10.4319/lo.2002.47.1.0266

Turnbull, L., Wainwright, J., & Brazier, R. E. (2008). A conceptual framework for understanding semi-arid land degradation: ecohydrological interactions across multiple-space and time scales. *Ecohydrology*, *1*(1), 23–34. https://doi.org/10.1002/eco.4

Ward, A. S., Fitzgerald, M., Gooseff, M. N., Voltz, T. J., Binley, A. M., & Singha, K. (2012). Hydrologic and geomorphic controls on hyporheic exchange during base flow recession in a headwater mountain stream. *Water Resources Research*, *48*(4).

Ward, J. V. (1989). The Four-Dimensional Nature of Lotic Ecosystems Author (s): J . V . Ward Source : Journal of the North American Benthological Society , Vol . 8 , No . 1 (Mar ., 1989), Published by : The University of Chicago Press on behalf of the Society for Freshwa. *Journal of the North American Benthological Society*, *8*(1), 2–8.

Westbrook, C. J., Cooper, D. J., & Baker, B. W. (2011). Beaver assisted river valley formation. *River Research and Applications*, *27*(2), 247–256. https://doi.org/10.1002/rra.1359

Wohl, E., Lininger, K. B., & Scott, D. N. (2017). River beads as a conceptual framework for building carbon storage and resilience to extreme climate events into river management. *Biogeochemistry*, 1–19. https://doi.org/10.1007/s10533-017-0397-7

Wohl, E., Brierley, G., Cadol, D., Coulthard, T. J., Covino, T., Fryirs, K. A., … Sklar, L. S. (2019). Connectivity as an emergent property of geomorphic systems. *Earth Surface Processes and Landforms*, *44*(1), 4–26. https://doi.org/10.1002/esp.4434

Table 1: Results of high and low flow conservative tracer injections. NaCl was injected 125m above Inflow, the source location, and monitored at the 6 target sites listed in the "Target Site" column. NR indicates that no tracer arrival was observed at the target site. There was no observed surface water connection between Inflow (the source) and Pond-Iso, but there were observed surface water connections between Inflow and the remaining 5 sites listed for at least part of the study period (May – October 2018).

					High Flow (June 13, 2018)		Low Flow (July 30, 2018)	
				Inflow Stage (mm:):	635		384	
Target Site	Site Type	Elev (m)	Surface Connection to Inflow	DISTf[1] (m)	TTP[2] (min)	Vmod[3] (m/s)	TTP[2] (min)	Vmod[3] (m/s)
Outflow	Major Channel	2535	Yes	2228	46	0.78	85	0.43
Main-Mid	Major Channel	2543	Yes	1175	23	0.87	41	0.48
Side-01	Side Channel	2548	Yes	607	35	0.29	NR	NR
Pond-Con-01	Connected Pond	2542	Yes	1040	196	0.09	NR	NR
Pond-Con-02	Connected Pond	2545	Yes	734	101	0.12	NR	NR
Pond-Iso	Isolated Pond	2550	No	-	NR	NR	NR	NR

1) Estimated surface flow path distance from the injection site. Note there is no surface channel connection between Inflow and the Isolated Pond (Pond-Iso)
2) Time to Peak
3) Modal Velocity – calculated as DISTf / TTP

Table 2: Five years of modeled inter-annual variability in connectivity dynamics at intermittently connected target sites. We used data from 2018 to develop empirical models to simulate connectivity dynamics for 2016 to 2020. Duration refers to the % of the annual study period (May – September) spent in each connectivity range (High > 0.6, Intermediate: 0.4-0.6, and Low < 0.4). We define sensitivity at each site for each duration category as the difference between the maximum duration and minimum duration within the five years.

	High Connectivity Duration ($\sigma_m \geq 0.6$)		***Intermediate Connectivity Duration*** ($0.4 < \sigma_m > 0.6$)		***Low Connectivity Duration*** ($\sigma_m \leq 0.4$)	
Sitename	**Range (%)**	**Sensitivity (Max - Min)**	**Range (%)**	**Sensitivity (Max - Min)**	**Range (%)**	**Sensitivity (Max - Min)**
Main-Braid	71 - 90	19	10 - 26	16	0 - 10	10
Pond-Con-01	33 - 54	21	16 - 22	6	29 - 52	23
Pond-Con-02	16 - 34	18	5- 18	13	51 - 73	22
Side-01	33 - 54	21	15 -21	6	29 - 52	23
Side-02	26 - 42	16	11 - 20	9	40 - 63	23
Side-03	17 - 35	18	7 - 16	9	51 - 71	20
Side-04	11 - 33	22	5 - 18	13	55 - 73	18

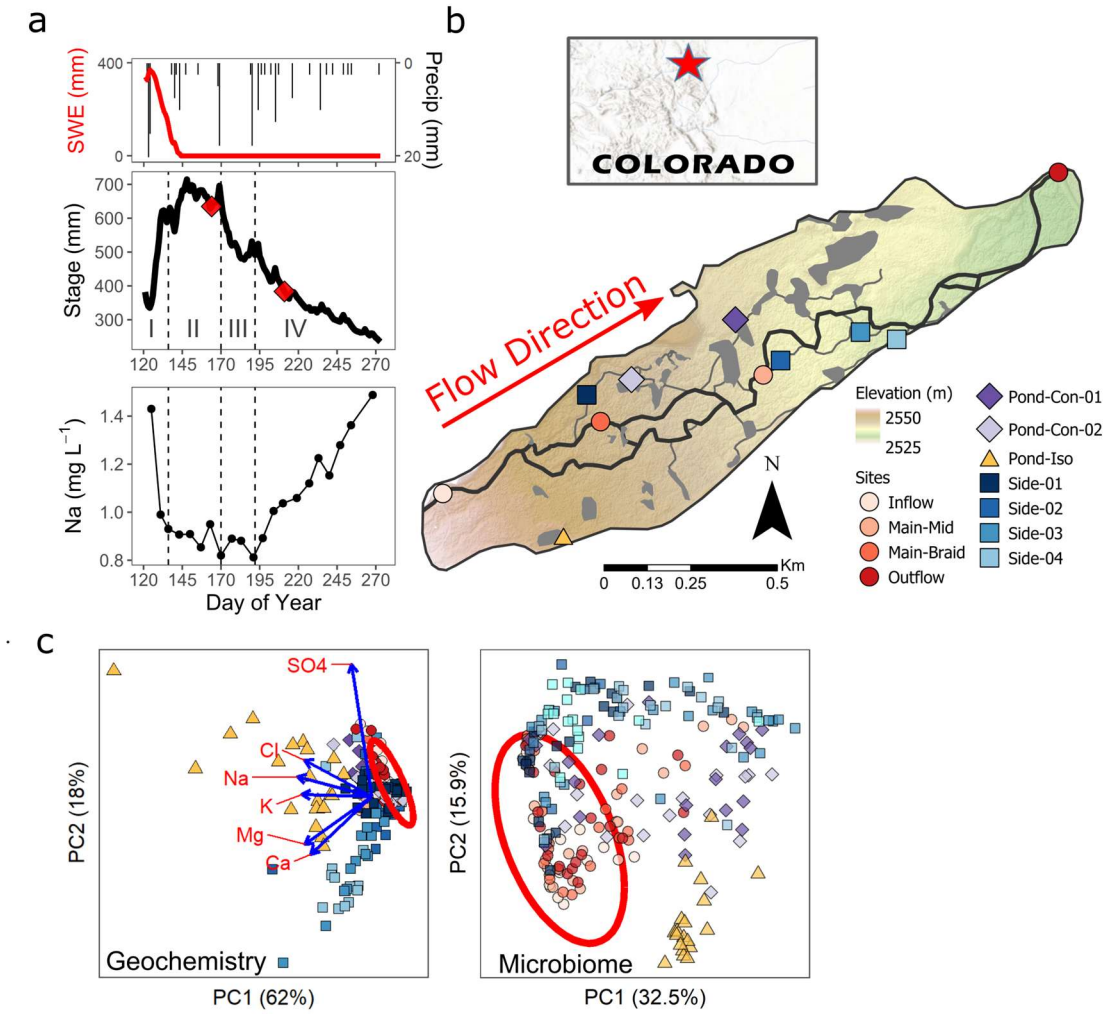

Figure 1: (a top) Precipitation and snow water equivalent (SWE) from SNOTEL #1042, (a middle) stage and (a bottom) sodium (Na) concentrations at Inflow, (b) North St Vrain river-floodplain map, and (c left) geochemical PCA and (c right) microbiome PCOAs showing full sampling dataset with axis labels indicating variance explained on each axiss. Red line in

(a top) is SWE) red diamonds in (a middle) indicate dates of tracer injection experiments. River flow hydro-periods in (a) are categorized as (I) rising limb, (II) peak flows, (III) falling limb, and (IV) recession. Map shows depiction of surface water major river braids (dark grey) and floodplain surface features including ponds, wetlands and side channels (lighter grey). Red circles in (c) are 90% confidence ellipses for Inflow site.

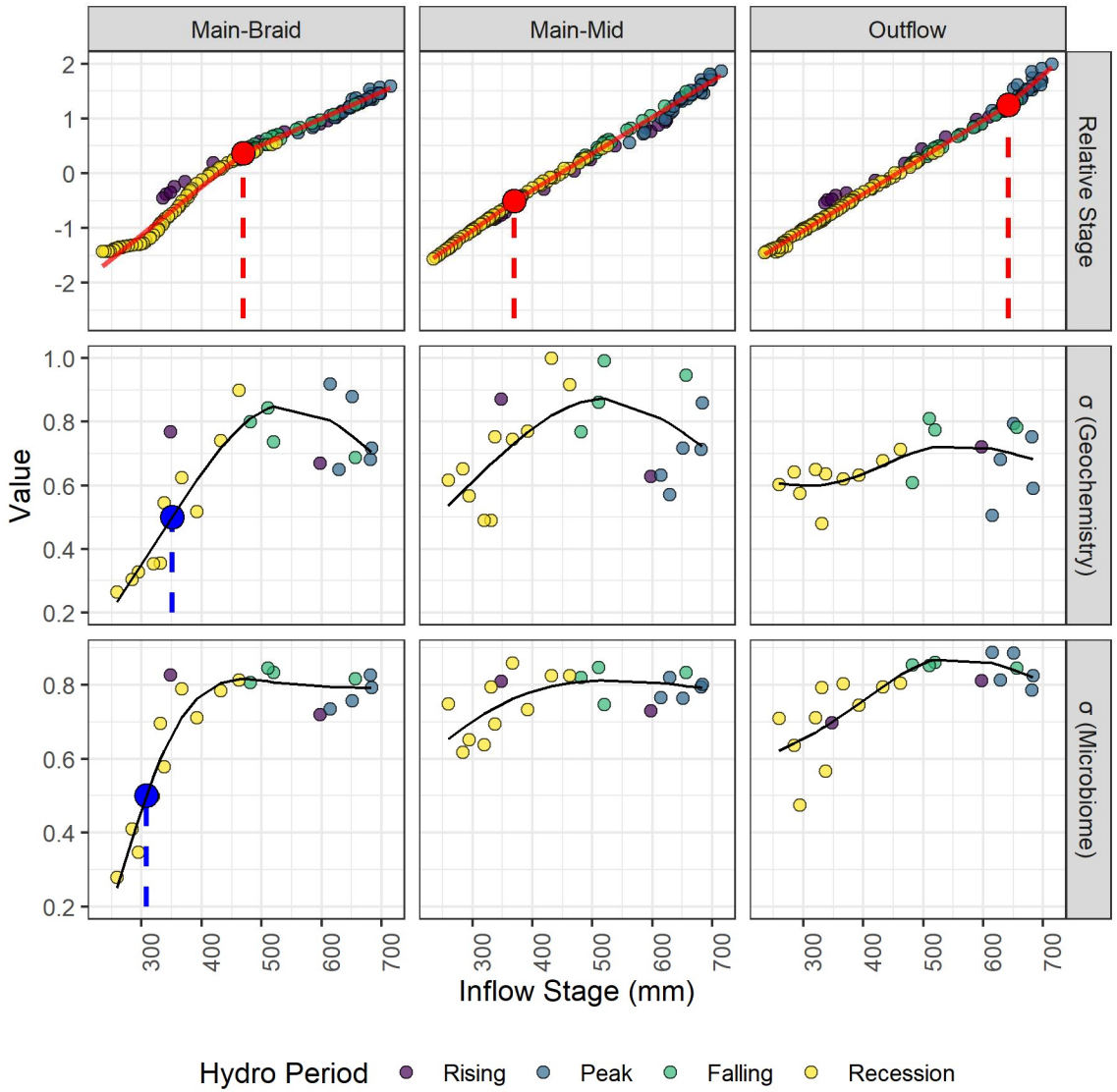
Main-Braid
Main-Mid
Outflow
Relative Stage
σ (Geochemistry)
σ (Microbiome)
Value
Inflow Stage (mm)
Hydro Period
Rising
Peak
Falling
Recession

30

Figure 2: Source-target relationships between Inflow stage and major channel target sites for relative stage (i.e., stage z-score, top row), geochemistry connectivity strength (middle row), and microbiome connectivity strength (bottom row). Red lines in the top row are broken stick regression predictions, and red dots and dashed lines are the identified inflection points in the source-target stage relationships. Black lines in the middle and bottom rows are the spline regression functions for connectivity strength metrics. Blue dots and dashed lines in middle and bottom rows are the Inflow stages at which connectivity strength functions are equal to 0.5. Missing blue dots/lines indicate that the connectivity strength function remained either above or below the 0.5 threshold for the duration of the study at that particular location.

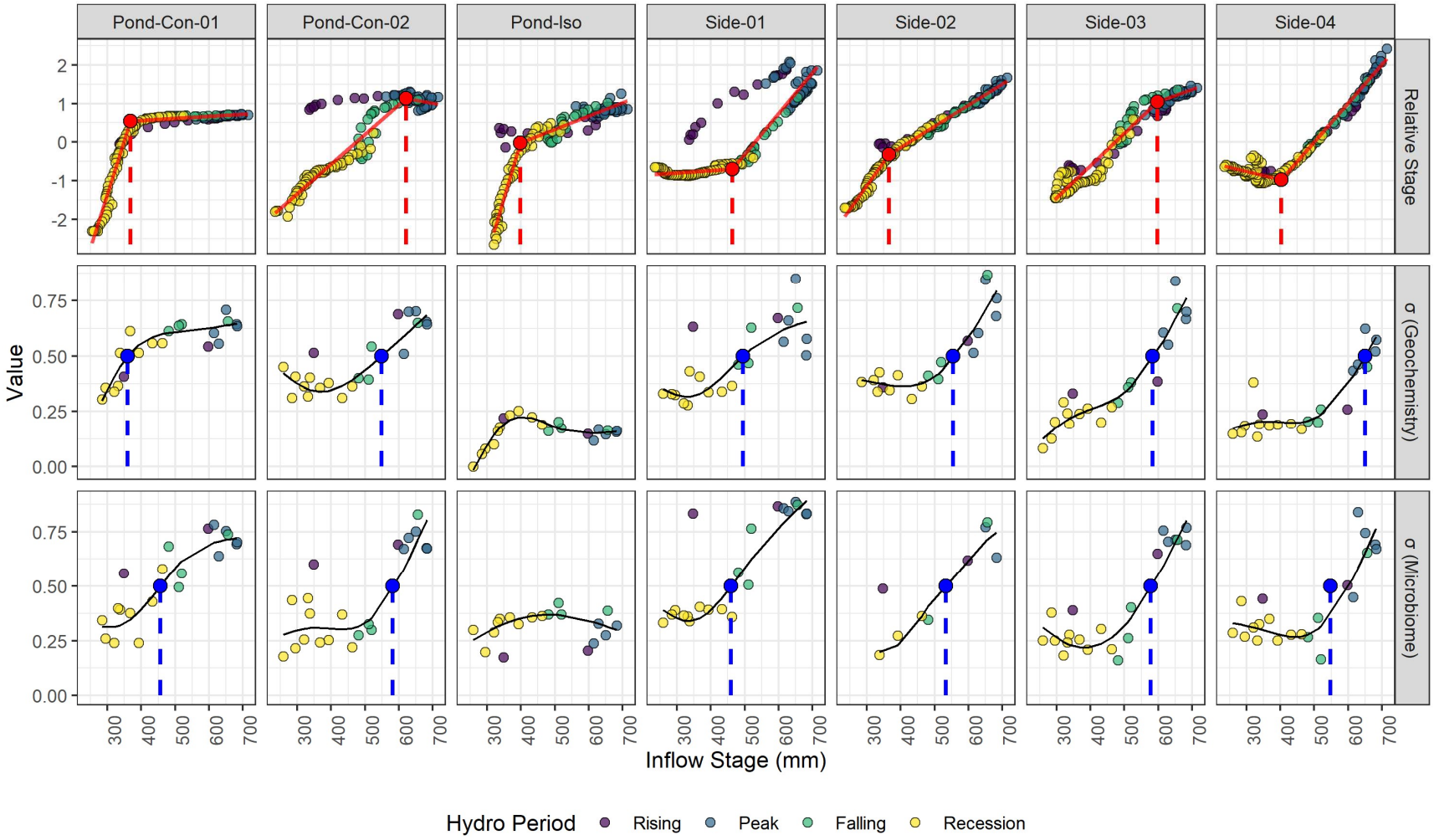

Figure 3: Source-target relationships between Inflow stage and floodplain target sites for relative stage (i.e., stage z-score, top row), geochemistry connectivity strength (middle row), and microbiome connectivity strength (bottom row). Red lines in the top row are broken stick regression predictions, and red dots and dashed lines are the identified inflection points in the source-target stage relationships. Black lines in the middle and bottom rows are the spline regression functions for

connectivity strength metrics. Blue dots and dashed lines in middle and bottom rows are the Inflow stages at which connectivity strength functions are equal to 0.5. Missing blue dots/lines indicate that the connectivity strength function remained either above or below the 0.5 threshold for the duration of the study at that particular location.

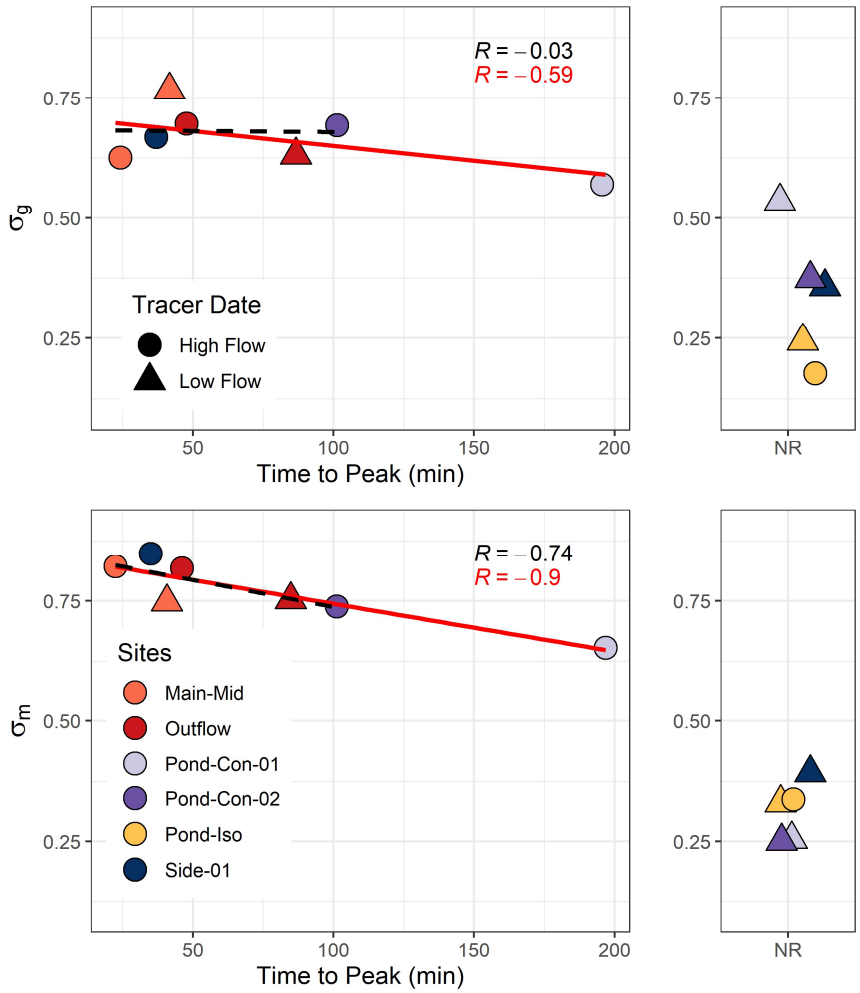

Figure 4: Connectivity strength metric validation with tracer response and time to peak in minutes (TTP), including results from both high (circle) and low (triangle) flow tracer injections (see Table 1 for tracer injection details). The left panels show sites and dates where we observed tracer arrival. Conversely, the right panels show sites and dates where there

was no observed tracer arrival. The x-axis of the left panels is the time to the peak of the injected tracer breakthrough curve, and NR on the x-axis of the right panels indicates no response (i.e., there was no observed arrival of injected tracer). Pearson correlation coefficients were calculated between connectivity strength and TTP both including (red) and not including (black) Pond-Con-01 high flow tracer response due to high leverage of that point. Both connectivity strength metrics distinguished well between sites with and without responses. The microbiome connectivity metric (σ_m) correlated more strongly with TTP.

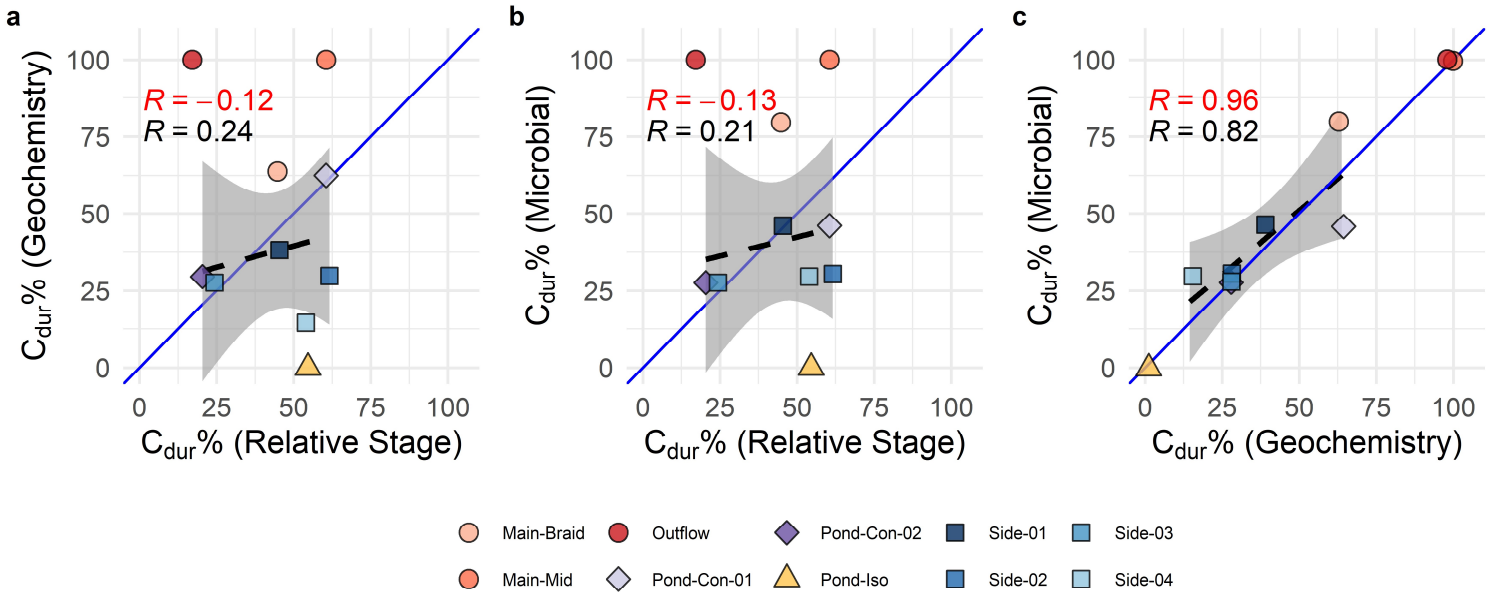

Figure 5: Connectivity duration (C_{dur}) at each site (as percent of 2018 study period) comparison as calculated with a) relative stage and geochemistry connectivity strength, b) relative stage and microbial connectivity strength and c) geochemistry and microbial connectivity strength. Blue solid line is 1:1 line. Pearson correlation coefficients (R) were calculated for all sites (shown in red font) and in (a) and (b) also with stable sites (Outflow, Main-Mid & Pond-Iso) excluded (shown in black font). Best fit line (black, dashed) shown excludes stable sites. Connectivity duration derived from relative stage is weakly correlated with other metrics while the two connectivity strength metrics are strongly correlated with each other.

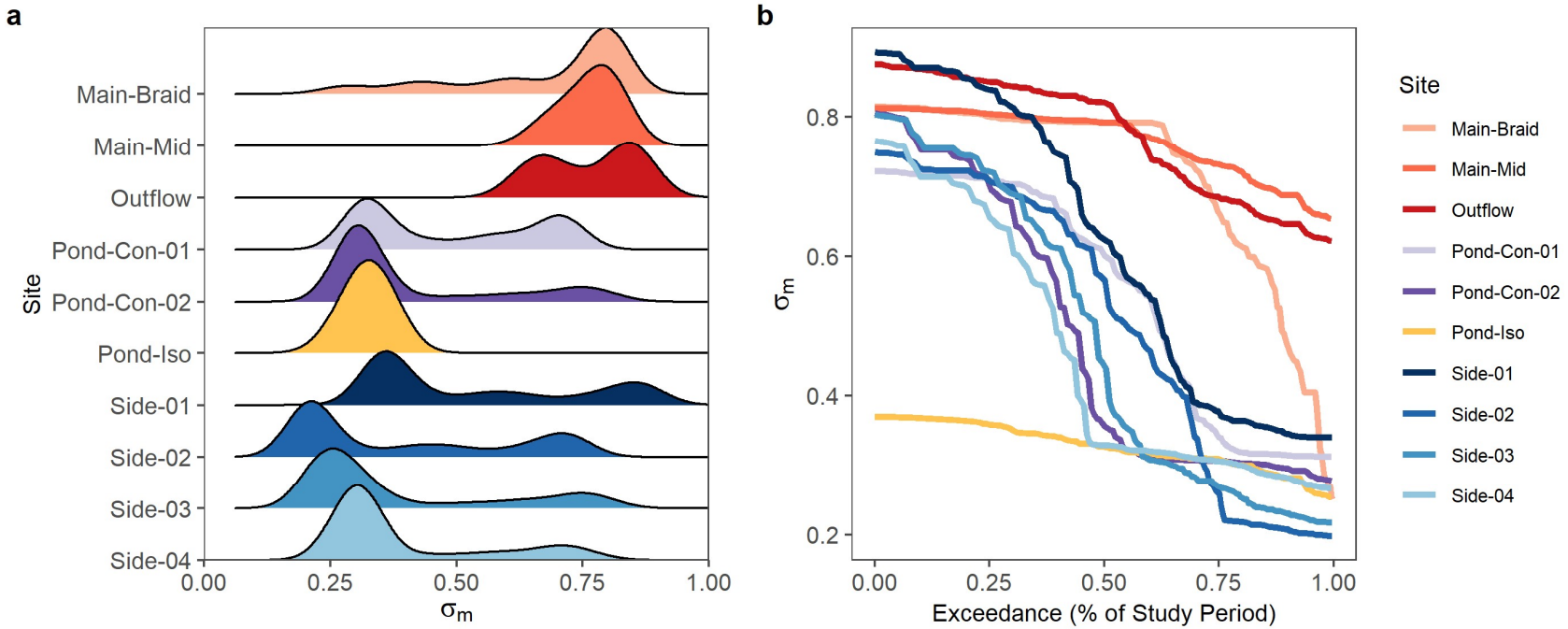

Figure 6: Target site-specific connectivity distributions during 2018 study period based on modeled daily microbiome connectivity strength (σ_m). a) Kernel density plots of σ_m. b) Empirical duration curves of σ_m. Sites with stable connectivity exhibit small spread in kernel density plots, while most intermittently connected sites exhibited high spread and a dominant mode at low connectivity strength values. Some intermittently connected sites had moderate durations at intermittent connectivity strengths while other sites exhibit rapid shifts between high and low strength values, demonstrated by the slope of lines in panel b.

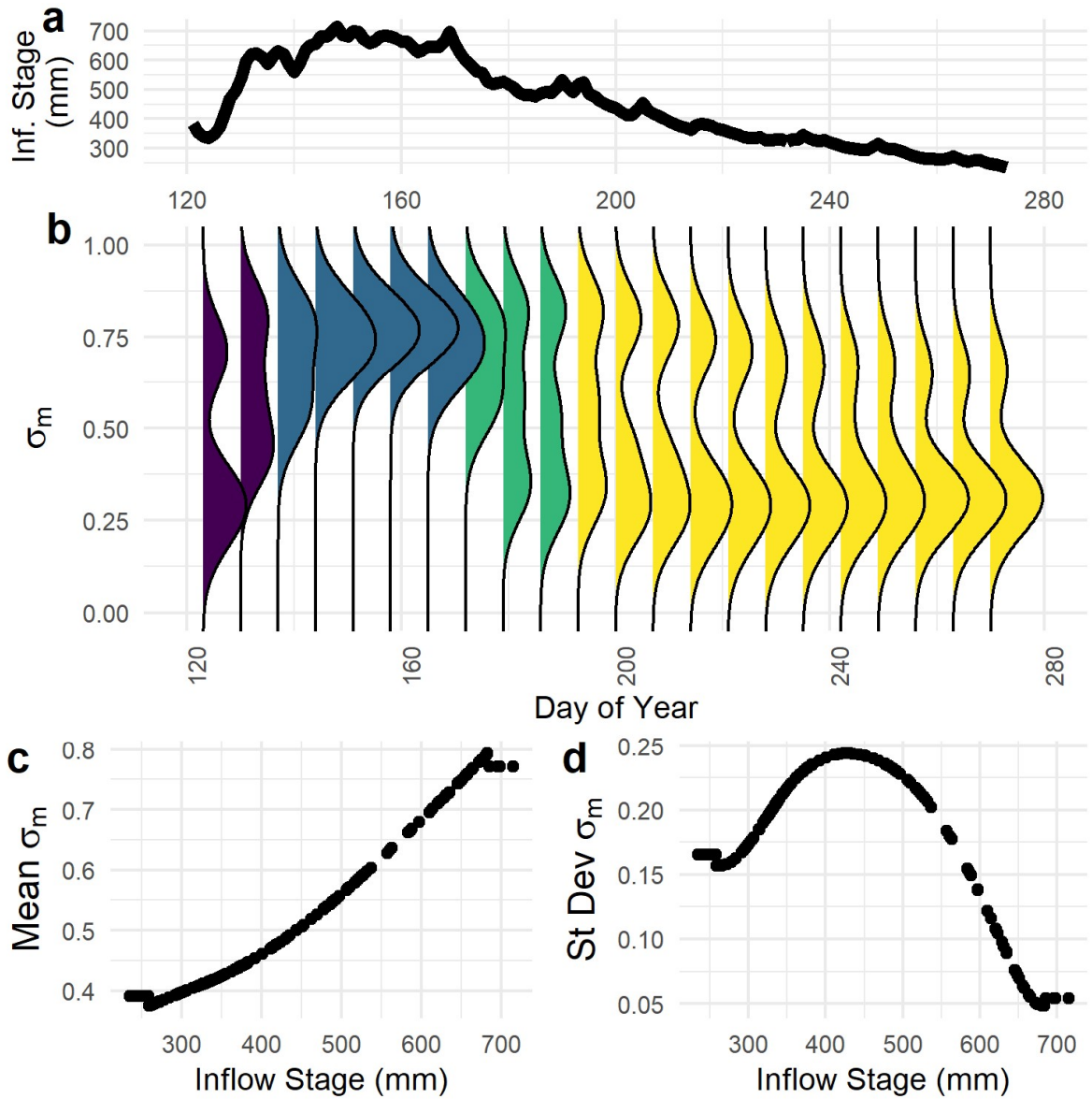
a
Inf. Stage (mm)
700
600
500
400
300
120
160
200
240
280
b
1.00
0.75
0.50
0.25
0.00
σm
120
160
200
240
280
Day of Year
c
Mean σm
0.8
0.7
0.6
0.5
0.4
300
400
500
600
700
Inflow Stage (mm)
d
St Dev σm
0.25
0.20
0.15
0.10
0.05
300
400
500
600
700
Inflow Stage (mm)

79

Figure 7: Aggregated system scale connectivity dynamics for 2018 study period using modeled daily connectivity strength (σ_m). a) Inflow stage. b) Kernel density of weekly mean σ_m for sites (excluding Pond-Iso) colored by hydro period: rising (purple), peak (blue), falling (green), and recession (yellow). c) Relationship between daily system mean σ_m and Inflow stage. d) Relationship between daily standard deviation of σ_m across the river-floodplain system as a function of Inflow stage. Connectivity strength is derived from microbiomes in all plots. Mean system connectivity increases continuously with Inflow stage while variation in system connectivity peaks at moderate Inflow stages. Flat lines in (c) and (d) at very low and high values are boundary effects caused by making predictions outside the range of Inflow stages that were sampled during study period.

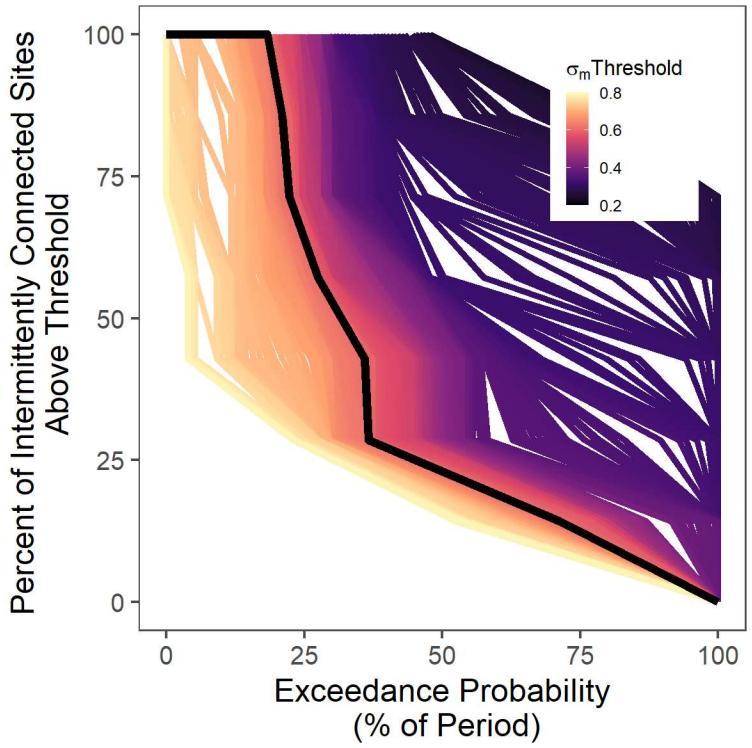

Figure 8: Aggregated river-floodplain system scale connectivity in 2018 across variable connectivity strength (σ_m) thresholds. The threshold is varied between the 10^{th} to 90^{th} percentiles of σ_m. Connectivity strengh is calculated with the microbiome metric. Only sites with an observed intermittent connectivity regime in 2018 were included (7 of the 10 target sites). Black line represent 0.5 σ_m threshold value.

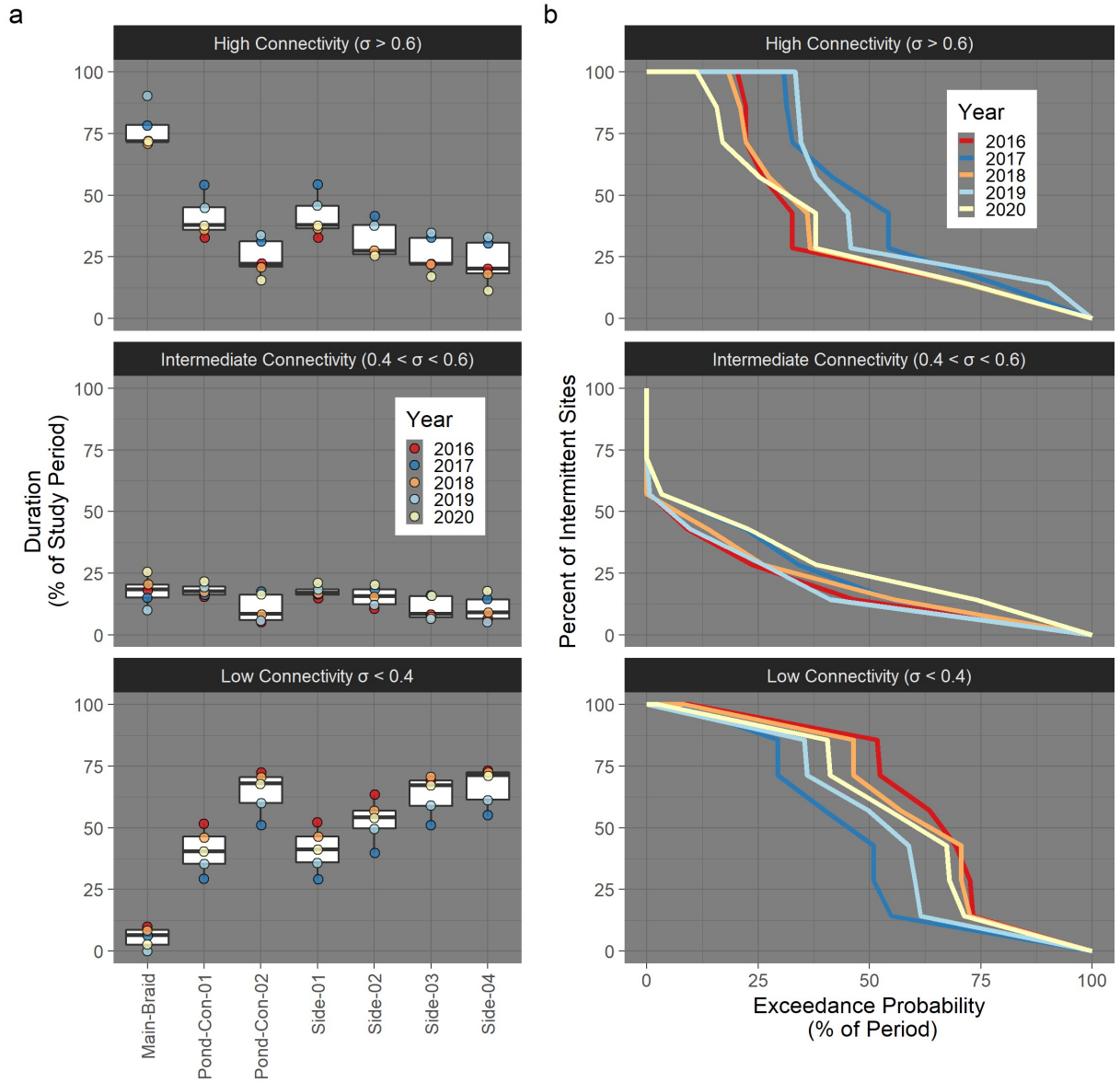
a
b
High Connectivity (σ > 0.6)
Intermediate Connectivity (0.4 < σ < 0.6)
Low Connectivity σ < 0.4
Low Connectivity (σ < 0.4)
Duration
(% of Study Period)
Percent of Intermittent Sites
Year
2016
2017
2018
2019
2020
0
25
50
75
100
Main-Braid
Pond-Con-01
Pond-Con-02
Side-01
Side-02
Side-03
Side-04
Exceedance Probability
(% of Period)

96

Figure 9: Interannual variability in river-floodplain connectivity for 2016 through 2020. Connectivity strength (σ_m) is predicted using 2018 site-specific models applied to observed Inflow stage records in each year. a) Boxplots of yearly duration of high, intermediate and low connectivity as percent of May-September study period. b) Exceedance probabilities of fraction of sites connected across the study period. Color for each year reflects annual wetness and is ordered from low (red) to high (blue) using annual median Inflow stage. Connectivity strengh is calculated using the microbiome metric and only sites with an observed intermittent connectivity regime in 2018 were included (7 of the 10 target sites). The duration of high and low connectivity were moderately sensitive to interannual streamflow varibility across all sites, generating substantial year to year variation in floodplain scale dynamics. The duration of intermediate connectivity was lower overall, and at several sites these durations were insensitive to inter-annual flow variation, resulting in less year to year variation in intermediate connectivity dyanmics across the river-floodplain system.

114

115

116

117

118

119

120

121